

Ultra-high frequency spikes of relic gravitons

Massimo Giovannini ¹

Department of Physics, CERN, 1211 Geneva 23, Switzerland

INFN, Section of Milan-Bicocca, 20126 Milan, Italy

Abstract

The maximal frequency domain of the cosmic gravitons falls in the THz region where, without conflicting with the existing phenomenological bounds, only few particles with opposite (comoving) three-momenta are produced. Although any reliable scrutiny of the ultra-high frequency spikes should include all the sources of late-time suppression at lower and intermediate frequencies, some relevant properties of the averaged multiplicities and of the spectral energy density can be derived within a reduced set of approximations that may become invalid as the frequency decreases well below the Hz. The accuracy of these concurrent approaches is assessed from the properties of the transition matrix that relates the late-time spectra to the values of the mode functions during an inflationary stage. In the obtained framework the bounds on the post-inflationary expansion rate are swiftly deduced and compare quite well with the ones including a more faithful numerical treatment. It also follows that the timeline of the post-inflationary expansion rate might be observationally accessible, in the years to come, provided the electromechanical detectors (like microwave cavities or waveguides) operating between the MHz and the THz shall eventually reach sensitivities in the chirp amplitudes which are (at least) twelve orders of magnitude smaller than the ones experimentally attainable in the audio band (i.e. between few Hz and the kHz).

arXiv:2503.12175v1 [gr-qc] 15 Mar 2025

¹e-mail address: massimo.giovannini@cern.ch

1 Introduction

The low frequency gravitational waves constrain the conventional inflationary scenarios through the relative weight of the tensor and scalar power spectra (denoted hereunder by r_T) at the conventional pivot scale k_p [1]. According to the available observational limits we should require that $r_T < 0.06$ [2, 3, 4] and since the frequency corresponding to $k_p = 0.002 \text{ Mpc}^{-1}$ is of the order of $\nu_p = 3.09 \text{ aHz}$ (where $1 \text{ aHz} = 10^{-18} \text{ Hz}$) the bounds on r_T ultimately constrain the low frequency spectral range of the relic gravitons (see, for instance, [5] for a review). Indeed, even before the formulation of the conventional inflationary paradigm it has been realized that any variation of the space-time curvature must produce shots of relic gravitons [6, 7] with different averaged multiplicities and slopes that faithfully reflect the early evolution of the background geometry. A standard timeline of the expansion rate would stipulate that an inflationary stage is followed by a radiation-dominated epoch so that, at the present conformal time τ_0 , the spectral energy density in critical units (denoted in what follows by $\Omega_{gw}(\nu, \tau_0)$) is quasi-flat for comoving frequencies ν approximately larger than 100 aHz [8, 9]; more specifically in this spectral domain we should have that $h_0^2 \Omega_{gw}(\nu, \tau_0) < \mathcal{O}(10^{-17})$ (where h_0 denotes, in what follows, the indetermination in the current value of the Hubble rate). In the concordance paradigm (possibly supplemented by an early stage of inflationary expansion) the spectral slope always decreases and thanks to the consistency relations, the tensor spectral index n_T is notoriously related to the tensor to scalar ratio r_T as $n_T \simeq -r_T/8$ [1, 2, 3, 4]. This conclusion can be however evaded provided the post-inflationary expansion rate is slower than radiation as originally suggested in Ref. [10]: in this case $\Omega_{gw}(\nu, \tau_0)$ may generically increase as a function of the comoving frequency. Depending on the timeline of the expansion rate, the presence of spikes may arise in various ranges either below the Hz or above it. Although the considerations discussed here may be applied to a number of physical situations, our examples primarily involve the presence of a single post-inflationary phase different from the radiation stage that may be recovered at a later (or even much later) epoch.

If the spectral energy density increases either in the intermediate or high frequency ranges, the expected signals in the MHz and GHz domains may even be eight orders of magnitude larger than the ones of the concordance paradigm [5, 10] and this is why electromechanical detectors are believed to be particularly suitable for the detection of high frequency gravitons. While the first detectors proposed at high frequencies consisted of toroidal waveguides with a propagating wavepacket of electromagnetic radiation [11, 12], also static electromagnetic fields (i.e. microwave cavities with superconducting walls) have been considered later on [13, 14, 15, 16, 17, 18]. The original prototypes could in principle resolve chirp amplitudes $h_c = \mathcal{O}(10^{-17})$ [13, 14, 15] and nearly twenty years later the sensitivities reached the level of $h_c = \mathcal{O}(10^{-20})$ [16, 17]. The minimal chirp amplitudes resolved by these detectors might be today comparable with the ones probed by wide-band interferometers in a much lower frequency range. In principle microwave cavities could detect relic gravitons between few GHz and 0.1 THz [18] but other devices have been suggested in similar ranges [19, 20, 21].

While the lowest frequency of the relic gravitons is ultimately determined by the current value of the Hubble rate, the maximal frequency apparently depends non-trivially on the specific scenario [22]. For instance in the concordance paradigm the maximal frequency turns out to be $\mathcal{O}(100) \text{ MHz}$ but this observation is purely academic: because of the steady decrease of the spectral energy density, the largest signal occurs anyway close to the pivot frequency $\nu_p = \mathcal{O}(\text{aHz})$. Absent any direct or indirect phenomenological indication on the post-inflationary history prior to the onset of big bang nucleosynthesis, the early timeline of the expansion rate may well be a sequel of arbitrary stages fulfilling certain reasonable constraints [23]. Broadly speaking, every phase expanding faster than radiation reduces the value of the maximal frequency below $\mathcal{O}(100) \text{ MHz}$ while the opposite is true for periods that expand less rapidly than radiation. If the expansion is slower than radiation for a sizeable portion of the post-inflationary evolution the maximal frequency may even exceed the GHz [22, 23]. The indetermination of the maximal frequency is related to the model dependence of the minimal wavelength below which the ultraviolet modes are never stretched by the inflationary expansion. Although the actual value of the maximal frequency depends upon the

timeline of the expansion rate, it is however possible to deduce a general bound that is independent on the specific scenario [22]. For this purpose we may observe that the spectral energy density in critical units ultimately depends on $\bar{n}(\nu, \tau_0)$ that denotes throughout the averaged multiplicity of the produced gravitons as a function of the (comoving) frequency:

$$\Omega_{gw}(\nu, \tau_0) = \frac{128 \pi^3}{3} \frac{\nu^4}{H_0^2 M_P^2} \bar{n}(\nu, \tau_0), \quad (1.1)$$

where H_0 is the current value of the Hubble rate and $M_P = 1/\sqrt{G}$ is the Planck mass² in the units adopted here (i.e. $\hbar = c = 1$); τ_0 denotes throughout the present value of the conformal time coordinate. Because of the unitarity of the process of graviton production, for $\nu > \nu_{max}$ the averaged multiplicity gets exponentially suppressed [24, 25] (see also [26, 27, 28, 29]) at a rate that depends on the smoothness of the transition. For $\nu > \nu_{max}$ the averaged multiplicity scales as $e^{-\gamma(\nu/\nu_{max})}$ where the value of γ is $\mathcal{O}(1)$ and can be concretely determined, for the specific scenario under consideration, with direct numerical integration as discussed in the past for the stochastic backgrounds of relic gravitational radiation [30]. Around the maximal frequency domain only few graviton pairs are produced and this means that in the limit $\nu \rightarrow \nu_{max}$ the averaged multiplicity $\bar{n}(\nu_{max}, \tau_0) = \mathcal{O}(1)$; from Eq. (1.1) the high frequency limits applicable to $\Omega_{gw}(\nu_{max}, \tau_0)$ can be translated into bounds on ν_{max} with the result that [22]

$$\nu_{max} < \mathcal{O}(0.1) \Omega_{R0}^{1/4} \sqrt{H_0 M_P} < \text{THz}, \quad (1.2)$$

where Ω_{R0} denotes throughout the current fraction of relativistic species in the plasma. In the minimal version of the concordance paradigm the neutrinos are often considered to be massless since they practically count as radiation when the initial conditions of CMB anisotropies are set; thus $h_0^2 \Omega_{R0}$ ranges in practice between 2.47×10^{-5} and 4.15×10^{-5} [1] (see also [2, 3, 4]). The difference between these figures is immaterial for the present ends but it should be borne in mind.

The careful evaluation of the spectrum of the relic gravitons must also include various sources of late-time suppression and in the concordance paradigm the spectral energy density is reduced by the transition to the dark energy, by the evolution of the relativistic species and, most notably, by the free-streaming of neutrinos [31, 32, 33, 34, 35]. The free-streaming is effective below the nHz, i.e. close to the typical frequency associated with big bang nucleosynthesis (see also [5] and discussions therein). While a rigorous and quantitative perspective is unavoidable (and has been thoroughly pursued in the relatively recent past) we intend to introduce here an approximate (but semi-analytic) discussion of the high frequency spike of the spectral energy density for two complementary reasons. In the first place simpler (but approximate) expressions are useful for the derivation of specific templates and are also relevant if we ought to set the accuracy of different approximation schemes. The second motivation is that, within one order of magnitude, the high frequency limits are independent on the damping effects occurring at smaller frequencies even though the late-time suppression does affect the overall normalization of the spectrum. This is the logic developed hereunder and the layout of the investigation is, in short, the following. In section 2 some of the technical aspects of the problem are outlined and briefly discussed with particular attention to the general form of the observables that are specifically analyzed and computed in the different sections of the paper. The evaluation of the high frequency spectrum is explored in section 3 within the Wentzel–Kramers–Brillouin (WKB) approach. In section 4 the spectra are instead deduced from the elements of a transition matrix relating the late-time values of the mode functions to the inflationary spectra. Even if, a posteriori, the latter strategy turns out to be more accurate than the former, in both cases the analysis involves generic post-inflationary expansion rates that do not necessarily coincide with radiation. Particular attention is paid to the case where the rate is slower than radiation and the underlying sources are maximally stiff. After a quantitative comparison of the different approaches, in section 5 the

²In this paper $M_P = 1/\sqrt{G}$ while $\bar{M}_P = 1/\sqrt{8\pi G}$ is the reduced Planck mass. Within the present notations we also introduce the Planck length $\ell_P = 1/\bar{M}_P$.

high and low frequency normalizations are compared both analytically and numerically. Once the bound of Eq. (1.2) is enforced the two strategies are fully compatible but the analytic discussion is swifter than the numerical one which is however intrinsically more accurate in the realistic situation. At the end of section 5 the typical values of the chirp amplitudes are discussed with few comments on the detectability strategies that often disregard the physical properties of the expected signals. Section 6 contains our concluding considerations.

2 Random backgrounds of relic gravitons

To avoid extended introductions that can be found elsewhere (see e.g. [22, 23]), we directly start from the Hamiltonian of the relic gravitons written in terms of the canonical fields $h_{ij}(\vec{x}, \tau)$ and of the corresponding canonical momenta $\pi_{ij}(\vec{x}, \tau)$

$$H_g(\tau) = \int d^3x \left[\frac{8\ell_P^2}{a^2(\tau)} \pi_{ij} \pi^{ij} + \frac{a^2(\tau)}{8\ell_P^2} \partial_k h_{ij} \partial^k h^{ij} \right], \quad (2.1)$$

where $\ell_P = \sqrt{8\pi G}$ and $a(\tau)$ is the scale factor of a spatially flat Friedmann-Robertson-Walker metric expressed as a function of the conformal time coordinate τ . Both $h_{ij}(\vec{x}, \tau)$ and $\pi_{ij}(\vec{x}, \tau)$ are solenoidal and traceless and describe the tensor inhomogeneities of the geometry. Furthermore Eq. (2.1) directly follows from the effective action discussed, with different strategies, in Refs. [36, 37] and since $H_g(\tau)$ is explicitly dependent upon the conformal time coordinate, all other Hamiltonians (possibly related to Eq. (2.1) via a time-dependent canonical transformation) are equally acceptable from the classical viewpoint but may lead to potential ambiguities at the quantum level. From Eq. (2.1) the evolution of $\pi_{ij}(\vec{x}, \tau)$ and $h_{ij}(\vec{x}, \tau)$ can be written as:

$$\partial_\tau h_{ij} = \frac{8\ell_P^2}{a^2(\tau)} \pi_{ij}, \quad \partial_\tau \pi_{ij} = \frac{a^2(\tau)}{8\ell_P^2} \nabla^2 h_{ij}. \quad (2.2)$$

We shall be generically considering hereunder a timeline of the curvature scale where a conventional inflationary stage precedes a phase of decelerated expansion which does not necessarily coincide with radiation. Therefore provided the inflationary epoch is long enough the classical inhomogeneities are suppressed and while the quantum fluctuations keep on reappearing all the time; $h_{ij}(\vec{x}, \tau)$ and $\pi_{ij}(\vec{x}, \tau)$ must then be associated with the appropriate Hermitian field operators:

$$\hat{h}_{ij}(\vec{x}, \tau) = \frac{\sqrt{2}\ell_P}{(2\pi)^{3/2}} \sum_\alpha \int d^3k e_{ij}^{(\alpha)}(\hat{k}) \left[\hat{b}_{\vec{k}, \alpha} F_{k, \alpha}(\tau) e^{-i\vec{k}\cdot\vec{x}} + \text{H. c.} \right], \quad (2.3)$$

$$\hat{\pi}_{ij}(\vec{x}, \tau) = \frac{a^2}{4\sqrt{2}\ell_P (2\pi)^{3/2}} \sum_\alpha \int d^3k e_{ij}^{(\alpha)}(\hat{k}) \left[\hat{b}_{\vec{k}, \alpha} G_{k, \alpha}(\tau) e^{-i\vec{k}\cdot\vec{x}} + \text{H. c.} \right]. \quad (2.4)$$

Both in Eqs. (2.3) and (2.4) ‘‘H.c.’’ indicates the Hermitian conjugate of the preceding term and the sum over α runs over the two tensor polarizations; if we introduce a triplet of unit vectors denoted, respectively, as $(\hat{m}, \hat{n}$ and \hat{k} with $\hat{m} \times \hat{n} = \hat{k}$) the two tensor polarizations are defined as $e_{ij}^{(\oplus)}(\hat{k}) = (\hat{m}_i \hat{m}_j - \hat{n}_i \hat{n}_j)$ and $e_{ij}^{(\otimes)}(\hat{k}) = (\hat{m}_i \hat{n}_j - \hat{n}_i \hat{m}_j)$. The commutation relations between the creation and annihilation operators are defined for a continuum of momenta, i.e. $[\hat{b}_{\vec{k}, \alpha}, \hat{b}_{\vec{p}, \beta}^\dagger] = \delta_{\alpha\beta} \delta^{(3)}(\vec{k} - \vec{p})$. Finally, the mode functions $F_{k, \alpha}$ and $G_{k, \alpha}$ introduced in Eqs. (2.3)–(2.4) can be rescaled at wish; a useful parametrization is $a F_{k, \alpha} = f_{k, \alpha}$ and $a G_{k, \alpha} = g_{k, \alpha}$. Thus the evolution of $F_{k, \alpha}$ and $G_{k, \alpha}$ follows directly from $f_{k, \alpha}$ and $g_{k, \alpha}$ since the scale factor will always be explicitly continuous with its first derivative; the equations obeyed by $f_{k, \alpha}$ and $g_{k, \alpha}$ follows by inserting Eqs. (2.3)–(2.4) into Eq. (2.2):

$$f'_k = g_k + \mathcal{H} f_k, \quad g'_k = -\mathcal{H} g_k - k^2 f_k, \quad \mathcal{H} = a'/a. \quad (2.5)$$

In Eq. (2.5) the prime denotes a derivation with respect to the conformal time coordinate τ and the index α has been suppressed since the same equations hold for both polarizations. The field operators of Eqs. (2.3)–(2.4) can also be represented in Fourier space

$$\widehat{h}_{ij}(\vec{k}, \tau) = \frac{1}{(2\pi)^{3/2}} \int d^3x \widehat{h}_{ij}(\vec{x}, \tau) e^{i\vec{k}\cdot\vec{x}}, \quad \widehat{\pi}_{ij}(\vec{k}, \tau) = \frac{1}{(2\pi)^{3/2}} \int d^3x \widehat{\pi}_{ij}(\vec{x}, \tau) e^{i\vec{k}\cdot\vec{x}}. \quad (2.6)$$

From Eqs. (2.3)–(2.4) and (2.6) the commutation relations of the field operators at equal times become

$$[\widehat{h}_{ij}(\vec{q}, \tau), \widehat{\pi}_{mn}(\vec{p}, \tau)] = i \mathcal{S}_{ijmn}(\hat{q}) \delta^{(3)}(\vec{q} + \vec{p}), \quad (2.7)$$

where, as usual, $\mathcal{S}_{ijmn}(\hat{q}) = [p_{im}(\hat{q})p_{jn}(\hat{q}) + p_{in}(\hat{q})p_{jm}(\hat{q}) - p_{ij}(\hat{q})p_{mn}(\hat{q})]/4$ and $p_{ij}(\hat{q}) = (\delta_{ij} - \hat{q}_i \hat{q}_j)$ indicates the traceless projector. If the canonical form of the commutation relations (2.7) is to be preserved by the time evolution of the field operators (2.3)–(2.4), the mode functions are imperatively subjected to the Wronskian normalization condition

$$f_k(\tau) g_k^*(\tau) - f_k^*(\tau) g_k(\tau) = i. \quad (2.8)$$

In the discussion of sections 3 and 4 we are going to emphasize the roles of the condition (2.8) that must always be satisfied throughout all the stages of the dynamical evolution. In case the initial vacuum state is annihilated by $\widehat{a}_{\vec{k}, \alpha}$ the two-point functions of the field operators and of their time derivatives is:

$$\langle \widehat{h}_{ij}(\vec{k}, \tau) \widehat{h}_{mn}(\vec{p}, \tau) \rangle = \frac{2\pi^2}{k^3} P_T(k, \tau) \mathcal{S}_{ijmn}(\hat{k}) \delta^{(3)}(\vec{k} + \vec{p}), \quad (2.9)$$

$$\langle \partial_\tau \widehat{h}_{ij}(\vec{k}, \tau) \partial_\tau \widehat{h}_{mn}(\vec{p}, \tau) \rangle = \frac{2\pi^2}{k^3} Q_T(k, \tau) \mathcal{S}_{ijmn}(\hat{k}) \delta^{(3)}(\vec{k} + \vec{p}), \quad (2.10)$$

where $P_T(k, \tau)$ and $Q_T(k, \tau)$ are the two power spectra that depend, respectively, upon $F_k(\tau)$ and $G_k(\tau)$:

$$P_T(k, \tau) = \frac{4 \ell_P^2 k^3}{\pi^2} |F_k(\tau)|^2, \quad Q_T(k, \tau) = \frac{4 \ell_P^2 k^3}{\pi^2} |G_k(\tau)|^2. \quad (2.11)$$

While Eq. (2.11) defines the tensor power spectrum that is often employed in the analysis of the conventional inflationary scenarios, the energy and the momentum of the gravitational field cannot be generally localized and assuming the equivalence principle in its stronger formulation it is conceptually difficult to propose a unique, local and gauge-invariant definition of the gravitational energy density [38, 39, 40] (see also [41, 42, 43]). This problem is particularly acute in the case of the relic gravitons since different strategies to assign the energy-momentum pseudo-tensor lead to a variety of problems especially for typical wavelengths larger than the Hubble radius [44]. Although there exist different and competing expressions for the energy-momentum pseudo-tensor of the gravitational field (see e.g. [38, 39, 40, 41, 42, 43]), not all of them satisfy the physical requirements that should be reasonably imposed in the case of the relic gravitons [44]. It follows however that a consistent expression for the energy-momentum tensor of the gravitational field can be derived from the variation of the second-order action [36, 37] with respect to the background geometry [44]

$$T_\mu^{(gw)\nu} = \frac{1}{4 \ell_P^2 a^2} \left[\partial_\mu h_{ij} \partial^\nu h^{ij} - \frac{1}{2} \delta_\mu^\nu \bar{g}^{\alpha\beta} \partial_\alpha h_{ij} \partial_\beta h^{ij} \right], \quad (2.12)$$

as suggested long ago by Ford and Parker [36]. From Eq. (2.12) we can then deduce the energy density of the relic gravitons which is given by:

$$\rho_{gw} = \frac{1}{8 \ell_P^2 a^2} \left[\partial_\tau h_{ij} \partial_\tau h^{ij} + \partial_k h_{ij} \partial^k h^{ij} \right]. \quad (2.13)$$

If the result of Eq. (2.13) is now averaged with the help of Eqs. (2.9)–(2.10) we can get to the explicit expression of the spectral energy density in critical units

$$\Omega_{gw}(k, \tau) = \frac{1}{\rho_{crit}} \frac{d\langle \rho_{gw} \rangle}{d \ln k} = \frac{1}{24 H^2 a^2} \left[k^2 P_T(k, \tau) + Q_T(k, \tau) \right], \quad (2.14)$$

where $\rho_{crit} = 3 H^2 \overline{M}_P^2 \equiv 3 H^2 / \ell_P^2$ denotes the critical energy density. It should be mentioned, at this point, that there are other variables that are customarily employed for the description of the random backgrounds of gravitational radiation such as the chirp amplitude $h_c(k, \tau)$ or the spectral amplitude conventionally denoted by $S_h(k, \tau)$. While the chirp amplitude can be safely employed in all physical situations, we should stress that the diffuse backgrounds of cosmological origin are non stationary [45]. The lack of stationarity is ultimately reflected into the spectral energy density and in all the other observables adopted for the description of a relic signal. A relevant consequence of this class of observations is that the spectral amplitude cannot be used for a rigorous description of the signal. The spectral amplitude (determined, according to the Wiener-Khintchine theorem, by the Fourier transform of the autocorrelation function of the process) should be time-independent but, in the case of cosmic gravitons, it is not³.

3 Essentials of the WKB evaluation

Even if not strictly necessary, for a consistent WKB solution it is useful to recast Eq. (2.5) (subjected to the condition (2.8)) in a decoupled form:

$$f_k'' + [k^2 - a''/a] f_k = 0, \quad g_k = f_k' - \mathcal{H} f_k. \quad (3.1)$$

For $k^2 \gg |a''/a|$ the solutions of Eq. (3.1) are plane waves and, depending on the shape of $|a''/a|$, this regime may also correspond to the limits $\tau \rightarrow \pm\infty$ but this correspondence is not strictly necessary, at least in the first approximation. Conversely, for $k^2 \ll |a''/a|$ the solution of Eq. (3.1) can be obtained by first transforming Eq. (3.1) into an integral equation

$$f_k(\tau) = f_k(\tau_{ex}) \frac{a(\tau)}{a_{ex}} + g_k(\tau_{ex}) \frac{a(\tau)}{a_{ex}} \int_{\tau_{ex}(k)}^{\tau} \frac{a_{ex}^2}{a^2(\tau')} d\tau' - k^2 a(\tau) \int_{\tau_{ex}(k)}^{\tau} \frac{d\tau'}{a^2(\tau')} \int_{\tau_{ex}(k)}^{\tau'} a(\tau'') f_k(\tau'') d\tau'', \quad (3.2)$$

where $\tau_{ex}(k)$ indicates the time when the wavelength $2\pi/k$ exits the Hubble radius (during the inflationary stage); in practice $\tau_{ex}(k)$ is determined from the (approximate) equality $k^2 \simeq |a''/a|_{\tau_{ex}}$. Equation (3.2) can be iteratively solved and, for instance, the first iteration consists in neglecting the term that contains k^2 that are effectively subleading when the relevant wavelengths are larger than the Hubble radius. The value of $g_k(\tau)$ can be either computed from $g_k = (f_k' - \mathcal{H} f_k)$ through Eq. (3.2) or it can be directly obtained from the decoupled evolution of $g_k(\tau)$, i.e. $g_k'' + [k^2 - a(1/a)''] g_k = 0$. In both approaches the values of $f_k(\tau_{ex})$ and $g_k(\tau_{ex})$ must comply with the Wronskian normalization condition (2.8) applied at $\tau_{ex}(k)$, i.e.

$$f_k(\tau_{ex}) g_k^*(\tau_{ex}) - f_k^*(\tau_{ex}) g_k(\tau_{ex}) = i. \quad (3.3)$$

Finally, the solutions in the regime $k^2 \gg |a''/a|$ and $k^2 \ll |a''/a|$ can be matched at $\tau_{ex}(k)$ and this procedure leads to a sound approximation for typical wavelengths larger than the Hubble radius.

3.1 The mode functions in the WKB approach

We are ultimately interested in the solution valid for wavelengths that have already reentered the Hubble radius at the present time. Indeed the validity of the approximation scheme leading to Eq. (3.2) stops

³While these issues have been recently discussed at length in [45], for the present ends the spectral energy density in critical units and the chirp amplitude will be the preferred variables; we shall therefore avoid using the spectral amplitude.

at $\tau_{re}(k)$, i.e. at the approximate time scale where a given wavelength reenters the Hubble radius; the solutions for the mode functions in the range $\tau > \tau_{re}(k)$ are again standing waves and can be written in the form:

$$f_k(\tau) = \frac{e^{-ik\tau_{ex}}}{\sqrt{2k}} \left[\mathcal{M}_k(\tau_{ex}, \tau_{re}) \cos k \Delta\tau + \mathcal{N}_k(\tau_{ex}, \tau_{re}) \sin k \Delta\tau \right], \quad (3.4)$$

$$g_k(\tau) = e^{-ik\tau_{ex}} \sqrt{\frac{k}{2}} \left[-\mathcal{M}_k(\tau_{ex}, \tau_{re}) \sin k \Delta\tau + \mathcal{N}_k(\tau_{ex}, \tau_{re}) \cos k \Delta\tau \right], \quad (3.5)$$

where $\Delta\tau = [\tau - \tau_{re}(k)]$. The explicit form of the functions $\mathcal{M}_k(\tau_{ex}, \tau_{re})$ and $\mathcal{N}_k(\tau_{ex}, \tau_{re})$ follows from the approximate solution (3.2) together with the requirement that the initial conditions in the limit $\tau \rightarrow -\infty$ are represented by travelling waves that obey the Wronskian normalization condition. The approximate solutions must then be continuously matched in $\tau_{ex}(k)$ and $\tau_{re}(k)$ by always bearing in mind the condition (3.3) which also constrain the explicit form of $\mathcal{M}_k(\tau_{ex}, \tau_{re})$ and $\mathcal{N}_k(\tau_{ex}, \tau_{re})$. The result of this lengthy but straightforward procedure is:

$$\mathcal{M}_k(\tau_{ex}, \tau_{re}) = \left(\frac{a_{re}}{a_{ex}} \right) Q_k(\tau_{ex}, \tau_{re}), \quad (3.6)$$

$$\mathcal{N}_k(\tau_{ex}, \tau_{re}) = \left(\frac{\mathcal{H}_{re}}{k} \right) \left(\frac{a_{re}}{a_{ex}} \right) Q_k(\tau_{ex}, \tau_{re}) - \left(\frac{a_{ex}}{a_{re}} \right) \left(\frac{\mathcal{H}_{ex} + ik}{k} \right), \quad (3.7)$$

$$Q_k(\tau_{ex}, \tau_{re}) = 1 - (\mathcal{H}_{ex} + ik) \int_{\tau_{ex}}^{\tau_{re}} \frac{a_{ex}^2}{a^2(\tau')} d\tau', \quad (3.8)$$

where $a_{re} = a(\tau_{re})$, $a_{ex} = a(\tau_{ex})$ while the other quantities, with obvious notations, are:

$$\mathcal{H}_{re} = \mathcal{H}(\tau_{re}) = a_{re} H_{re}, \quad \mathcal{H}_{ex} = \mathcal{H}(\tau_{ex}) = a_{ex} H_{ex}, \quad \mathcal{F}(\tau_{ex}, \tau_{re}) = \int_{\tau_{ex}(k)}^{\tau_{re}(k)} \frac{a_{ex}^2}{a^2(\tau)} d\tau. \quad (3.9)$$

It can be directly checked that the Wronskian normalization condition (2.8) is always satisfied by Eqs. (3.4)–(3.5) provided $\mathcal{M}_k(\tau_{ex}, \tau_{re})$ and $\mathcal{N}_k(\tau_{ex}, \tau_{re})$ have exactly the form given in Eqs. (3.6)–(3.7) and (3.8). If Eqs. (3.4)–(3.5) are inserted into Eqs. (2.10)–(2.11) and (2.14) it turns out that the spectral energy density in critical units depends on $|\mathcal{M}_k(\tau_{ex}, \tau_{re})|^2$ and $|\mathcal{N}_k(\tau_{ex}, \tau_{re})|^2$:

$$\Omega_{gw}(k, \tau) = \frac{2k^4}{3\pi H^2 a^4 M_P^2} \left[\left| \mathcal{M}_k(\tau_{ex}, \tau_{re}) \right|^2 + \left| \mathcal{N}_k(\tau_{ex}, \tau_{re}) \right|^2 \right]. \quad (3.10)$$

If we now insert Eqs. (3.6)–(3.7) into Eq. (3.10) the explicit form of $\Omega_{gw}(k, \tau)$ becomes:

$$\begin{aligned} \Omega_{gw}(k, \tau) &= \frac{2k^4}{3\pi H^2 a^4 M_P^2} \left\{ \left(\frac{a_{re}}{a_{ex}} \right)^2 \left(1 + \frac{\mathcal{H}_{re}^2}{k^2} \right) \left[1 + (\mathcal{H}_{ex}^2 + k^2) \mathcal{F}^2(\tau_{ex}, \tau_{re}) - 2\mathcal{H}_{ex} \mathcal{F}(\tau_{ex}, \tau_{re}) \right] \right. \\ &\quad \left. - 2 \frac{\mathcal{H}_{re}}{k} \left[\frac{\mathcal{H}_{ex}}{k} - \frac{\mathcal{H}_{ex}^2 + k^2}{k} \mathcal{F}(\tau_{ex}, \tau_{re}) \right] + \left(\frac{a_{ex}}{a_{re}} \right)^2 \left[1 + \frac{\mathcal{H}_{ex}^2}{k^2} \right] \right\}. \end{aligned} \quad (3.11)$$

In connection with Eq. (3.11) there are two important observations. The first one is that $\mathcal{H}_{ex} \simeq k$ at least as long as the exit of the given wavelength occurs during an inflationary stage of expansion (see however some exceptions described at the end of this subsection). The second observation is that there is a hierarchy between the first and the last terms of Eq. (3.11) implying that the first term always dominates against the last one: if the scale factor expands $a_{re} \gg a_{ex}$ so that the term containing $(a_{re}/a_{ex})^2$ is always negligible for all practical purposes. Thanks to these two remarks Eq. (3.11) can be rewritten as:

$$\begin{aligned} \Omega_{gw}(k, \tau) &= \frac{2k^4}{3\pi H^2 a^4 M_P^2} \left\{ \left(\frac{a_{re}}{a_{ex}} \right)^2 \left(1 + \frac{\mathcal{H}_{re}^2}{k^2} \right) \left[1 + 2k^2 \mathcal{F}^2(\tau_{ex}, \tau_{re}) \right. \right. \\ &\quad \left. \left. - 2k \mathcal{F}(\tau_{ex}, \tau_{re}) \right] - 2 \frac{\mathcal{H}_{re}}{k} \left[1 - 2k \mathcal{F}(\tau_{ex}, \tau_{re}) \right] \right\}. \end{aligned} \quad (3.12)$$

The values of $\tau_{ex}(k)$ and $\tau_{re}(k)$ define the change of the solution and are therefore the two turning points of the WKB approximation. From Eq. (3.1) the turning points approximately obey $k^2 \simeq |a''/a|$. The latter condition can also be written as $k^2 \simeq a^2 H^2 [2 - \epsilon]$ where $\epsilon = -\dot{H}/H^2$ and since during inflation $\epsilon \ll 1$ the turning point is always regular and, as anticipated, $k \simeq a_{ek} H_{ex} = \mathcal{H}_{ex}$. It can however happen that the reentry occurs either during the radiation stage or close to it: in this case $\epsilon = \mathcal{O}(2)$ and this implies that $k \ll a_{re} H_{re} = \mathcal{H}_{re}$. Thus when the reentry takes place during a radiation stage the terms $\mathcal{H}_{re}/k \gg 1$ dominate in Eq. (3.12).

3.2 Integrals for wavelengths larger than the Hubble radius

Within the WKB approach the high frequency normalization does not only depend upon the frequency slope but also on the evaluation of certain integrals whose numerical relevance may range between few percents and one order of magnitude. Although these contributions could simply be disregarded, for the sake of accuracy (and for a fair comparison with the results of section 5) we are now going to evaluate the integrals appearing in Eq. (3.12) by bearing in mind that they all involve a physical regime where the corresponding wavelengths are larger than the Hubble radius. Since for $\tau \rightarrow -\infty$ we assume an inflationary stage of expansion the (comoving) Hubble rate can be written as:

$$H a = -\frac{1}{(1 - \epsilon)\tau}, \quad \epsilon = -\dot{H}/H^2 \ll 1, \quad \tau \leq -\tau_1. \quad (3.13)$$

We then posit that for $\tau \geq -\tau_1$ there is a generic stage of decelerated expansion (i.e. $\delta > 0$)

$$H a = \frac{\delta}{\tau + \tau_1(1 + q)}, \quad q = q(\epsilon, \delta) = (1 - \epsilon)\delta, \quad \tau \geq -\tau_1. \quad (3.14)$$

If $\delta \rightarrow 1$ the background is dominated by radiation; conversely when $\delta \neq 1$ the expansion rate is, respectively, either slower (i.e. $\delta < 1$) or faster (i.e. $\delta > 1$) than radiation. Because of the presence of $q(\epsilon, \delta)$ in Eqs. (3.13)–(3.14) the scale factor and the expansion rate are explicitly continuous across the transition for any value of δ and ϵ . The integral $k \mathcal{F}(\tau_{ex}, \tau_{re})$ can then be separated into the two contributions preceding and following $-\tau_1$, namely:

$$k \mathcal{F}(\tau_{ex}, \tau_{re}) = k \int_{-1/k}^{-\tau_1} \frac{a_{ex}^2}{a^2(\tau)} d\tau + k \int_{-\tau_1}^{1/k} \frac{a_{ex}^2}{a^2(\tau)} d\tau. \quad (3.15)$$

Since the exit always occurs during the inflationary stage we can estimate a_{ex} as $a_{ex}^2 = (-\tau_{ex}/\tau_1)^{-2/(1-\epsilon)} \simeq |k\tau_1|^{2/(1-\epsilon)}$; therefore we have from Eq. (3.15) that

$$k \mathcal{F}(\tau_{ex}, \tau_{re}) = \frac{1}{p(\epsilon)} \left[1 - x_1^{p(\epsilon)} \right] + q^{2\delta} x_1^{2\delta+2/(1-\epsilon)} \int_{-x_1}^1 \frac{dx}{[x + (q+1)x_1]^{2\delta}}, \quad (3.16)$$

where the auxiliary quantity $p(\epsilon) = (3 - \epsilon)/(1 - \epsilon)$ has been introduced. Provided $\delta \neq 1/2$ we have that the whole integral appearing in Eq. (3.16) becomes

$$\begin{aligned} k \mathcal{F}(\tau_{ex}, \tau_{re}) &= \frac{1}{p(\epsilon)} \left[1 - x_1^{p(\epsilon)} \right] + \frac{q^{2\delta} x_1^{2\delta+2/(1-\epsilon)}}{1 - 2\delta} \left\{ \left[1 + (q+1)x_1 \right]^{1-2\delta} - \left(q x_1 \right)^{1-2\delta} \right\} \\ &= \frac{1}{p(\epsilon)} + \mathcal{O}\left(x_1^{3+2\epsilon}\right) + \mathcal{O}\left(x_1^{2\delta+2+2\epsilon}\right). \end{aligned} \quad (3.17)$$

In Eq. (3.17) all the corrections are subleading as long as $x_1 < 1$; this happens for all the wavenumbers smaller than the maximal one and for all the frequencies smaller than the maximal frequency. In the case

$\delta \rightarrow 1/2$ the evaluation is similar but the final result contains logarithmic corrections that can be estimated as follows:

$$k \mathcal{J}(\tau_{ex}, \tau_{re}) = \frac{1}{p(\epsilon)} - q x_1^{p(\epsilon)} \ln(q x_1). \quad (3.18)$$

We can now go back to Eq. (3.12) and note that the first term is always dominant in the case of an expanding background since it is proportional to $(a_{re}/a_{ex}) \gg 1$. This means that Eq. (3.12) can also be written as:

$$\Omega_{gw}(k, \tau) = \frac{2k^4}{3\pi H^2 a^4 M_P^2} \left(\frac{a_{re}}{a_{ex}}\right)^2 \left(1 + \frac{\mathcal{H}_{re}^2}{k^2}\right) \left[1 + 2k^2 \mathcal{J}^2(\tau_{ex}, \tau_{re}) - 2k \mathcal{J}(\tau_{ex}, \tau_{re})\right]. \quad (3.19)$$

3.3 The spectral energy density for different post-inflationary histories

The explicit expression of the spectral energy density will now be examined for different post-inflationary histories within the approximation schemes studied in this section. We first consider the situation where the given wavelength reenters the Hubble radius far from a radiation-dominated stage of expansion (i.e. $\epsilon_{re} \neq 2$); we furthermore require that $\delta \neq 1/2$ to avoid logarithmic corrections. From Eq. (3.19) we have

$$\Omega_{gw}(k, \tau) = \frac{2k^4 c_1(\epsilon)}{3\pi H^2 a^4 M_P^2} \left(\frac{a_{re}}{a_{ex}}\right)^2, \quad (3.20)$$

where the auxiliary constant $c_1(\epsilon)$ has been introduced and it is defined as:

$$c_1(\epsilon) = 2 \left[1 + \frac{2}{p^2(\epsilon)} - \frac{2}{p(\epsilon)}\right] = 2 \frac{[4 + (1 - \epsilon)^2]}{(3 - \epsilon)^2}. \quad (3.21)$$

As anticipated this factor comes from the integrals evaluated above but its actual numerical weight is $\mathcal{O}(1)$: in the limit $\epsilon \rightarrow 0$ we have that $c_1 \rightarrow 10/3$. We must then estimate explicitly $(a_{re}/a_{ex})^2$ in terms of Eqs. (3.13)–(3.14) and the result is:

$$\frac{a_{re}^2}{a_{ex}^2} = \frac{[(\tau_{re}/\tau_1 + 1)/q + 1]^{2\delta}}{(\tau_{ex}/\tau_1)^{-2/(1-\epsilon)}} = q^{-2\delta} \left(\frac{k}{a_1 H_1}\right)^{-2\delta - 2/(1-\epsilon)}. \quad (3.22)$$

For a concrete estimate of the spectral energy density of Eq. (3.20) we consider that the δ -phase of Eq. (3.14) extends between H_1 down to a curvature scale H_r marking the onset of the radiation-dominated stage. When $H < H_r$ the standard timeline of the concordance paradigm suggests that $3H_{eq}^2 \bar{M}_P^2 = 2\rho_{M0}(a_0/a_{eq})^3$ at the time of matter-radiation equality so that⁴ $(a_0/a_{eq}) = \Omega_{M0}/\Omega_{R0}$ where; with the same logic we can also compute $(a_0 H_0)/(a_{eq} H_{eq}) = (2\Omega_{R0})^{-1/4} \sqrt{H_0/H_{eq}}$. Since between H_r and H_{eq} the evolution is dominated by radiation we also have that

$$\left(\frac{a_{eq}^4 H_{eq}^2}{a_r^4 H_r^2}\right) = \frac{a_{eq}^4 T_{eq}^4 g_{\rho,eq}}{a_r^4 T_r^4 g_{\rho,r}} = \left(\frac{g_{\rho,eq}}{g_{\rho,r}}\right) \left(\frac{g_{s,r}}{g_{s,eq}}\right)^{4/3}. \quad (3.23)$$

In Eq. (3.23) g_ρ and g_s denote, respectively, the number of effective relativistic degrees of freedom appearing in the energy and entropy densities of the plasma. This simplified estimate follows by assuming local thermal equilibrium at H_r ; thus if the entropy density is conserved $g_{s,r} a_r^3 T_r^3 = g_{s,eq} a_{eq}^3 T_{eq}^3$ and this observation determines the redshift between the two epochs. In the standard situation where $g_{s,r} = g_{\rho,r} = 106.75$ and $g_{s,eq} = g_{\rho,eq} = 3.94$ so that difference due to g_s and g_ρ in the final results is actually negligible for the

⁴We recall that Ω_{R0} has been already introduced in Eq. (1.2) while Ω_{M0} is the critical fraction of matter in the concordance scenario

present purposes⁵. Thanks to Eqs. (3.20)–(3.22) and (3.23) we can therefore obtain the wanted estimate of $\Omega_{gw}(k, \tau)$ in the WKB approximation

$$\Omega_{gw}(k, \tau) = \frac{4 \Omega_{R0} c_1(\epsilon)}{3\pi q^{2\delta}} \left(\frac{H_1}{M_P}\right)^2 \left(\frac{H_r}{H_1}\right)^{\alpha(\delta)} \left(\frac{g_{\rho,r}}{g_{\rho,eq}}\right) \left(\frac{g_{s,eq}}{g_{sr}}\right)^{4/3} \left(\frac{k}{a_1 H_1}\right)^{n_T(\delta, r_T)}. \quad (3.24)$$

In Eq. (3.24) the spectral index $n_T(\delta, r_T)$ controls the slope of the spectral energy density while $\alpha(\delta)$ affects the overall amplitude of $\Omega_{gw}(k, \tau)$; the spectral index $n_T(\delta, r_T)$ and $\alpha(\delta)$ are given, respectively, by

$$n_T(\delta, r_T) = 4 - \frac{32}{16 - r_T} - 2\delta, \quad \alpha(\delta) = \frac{2(\delta - 1)}{\delta + 1}. \quad (3.25)$$

The result of Eq. (3.24) can be made even more explicit by recalling that $(H_1/M_P) = \sqrt{\pi \mathcal{A}_{\mathcal{R}} r_T}/4$:

$$\Omega_{gw}(k, \tau) = \frac{r_T \mathcal{A}_{\mathcal{R}} \Omega_{R0} c_1(\epsilon)}{12 q^{2\delta}} \left(\frac{H_r}{H_1}\right)^{\alpha(\delta)} \left(\frac{g_{\rho,r}}{g_{\rho,eq}}\right) \left(\frac{g_{s,eq}}{g_{sr}}\right)^{4/3} \left(\frac{k}{a_1 H_1}\right)^{n_T(\delta, r_T)}, \quad (3.26)$$

where $\mathcal{A}_{\mathcal{R}} = \mathcal{O}(10^{-9})$ denotes the amplitude of the scalar (i.e. curvature) inhomogeneities at the pivot scale k_p [1, 2, 3, 4]. The results of Eqs. (3.24) and (3.26) have been deduced in the case $\delta \neq 1/2$ but when $\delta \rightarrow 1/2$ the leading term is formally the same with the difference that $c_1(\epsilon, k)$ is now scale dependent:

$$\Omega_{gw}(k, \tau) = \frac{r_T \mathcal{A}_{\mathcal{R}} \Omega_{R0} c_1(\epsilon, k)}{12 q^{2\delta}} \left(\frac{H_r}{H_1}\right)^{\alpha(\delta)} \left(\frac{g_{\rho,r}}{g_{\rho,eq}}\right) \left(\frac{g_{s,eq}}{g_{sr}}\right)^{4/3} \left(\frac{k}{a_1 H_1}\right)^{n_T(1/2, r_T)}, \quad (3.27)$$

Two further auxiliary constants have been introduced in Eq. (3.27) and are defined as defined as:

$$\begin{aligned} c_1(\epsilon, k) &= 2 \frac{[4 + (1 - \epsilon)^2]}{(3 - \epsilon)^2} \left[1 + c_2(\epsilon) q \left(\frac{k}{a_1 H_1}\right)^{p(\epsilon)} \ln \left(\frac{k}{a_1 H_1}\right) \right], \\ c_2(\epsilon) &= \frac{2(3 + 2\epsilon - \epsilon^2)}{5 - 2\epsilon + \epsilon^2}. \end{aligned} \quad (3.28)$$

To complete the discussion we can finally deduce the spectral energy density when the reentry takes place in the radiation stage while the exit occurs, as usual, during an inflationary phase. In this situation we have that the conditions $\epsilon_{re} = \mathcal{O}(2)$ and $\epsilon_{ex} = \epsilon \ll 1$ imply that the exit is a regular turning point (i.e. $k \simeq a_{ex} H_{ex}$) while at reentry we would have instead $k^2 = a_{re}^2 H_{re}^2 [2 - \epsilon_{re}]$, i.e. $k \ll a_{re} H_{re}$. As already anticipated, the term $\mathcal{H}_{re}^2/k^2 \gg 1$ and from Eq. (3.20) we obtain:

$$\Omega_{gw}(k, \tau) = \frac{2 k^2 a_{re}^2 H_{re}^2 c_3(\epsilon)}{3 \pi H^2 a^4 M_P^2} \left(\frac{a_{re}}{a_{ex}}\right)^2, \quad (3.29)$$

where $c_3(\epsilon) = c_2(\epsilon)/2$ and in the limit $\epsilon \rightarrow 0$ $c_2 \rightarrow 6/5$. The dominant contribution written in Eq. (3.29) now follows from $\mathcal{H}_{re}^2/k^2 \gg 1$; for a more direct evaluation $\Omega_{gw}(k, \tau)$ can be written as:

$$\Omega_{gw}(k, \tau) = \frac{2 c_3(\epsilon)}{3 \pi} \left(\frac{k^2}{a_{ex}^2 H_{ex}^2}\right) \left(\frac{H_{ex}}{M_P}\right)^2 \frac{a_{re}^4 H_{re}^2}{a^4 H^2}, \quad (3.30)$$

where the right-hand side has been multiplied and divided by H_{ex}^2 . Since $k \simeq a_{ex} H_{ex}$, Eq. (3.30) further simplifies: the second term is of order 1 while $H_{ex}^2 = H_1^2 |k/(a_1 H_1)|^{\bar{n}_T}$ where, in this case, we denote $\bar{n}_T = -2\epsilon/(1 - \epsilon) \simeq -2\epsilon$. Since the consistency relations have been enforced throughout the discussion

⁵The difference due to g_s and g_ρ in the final results is actually involves a factor 1.3 (instead of 1) at the level of Eq. (3.23).

$\bar{n}_T = -2\epsilon \simeq -r_T/8$. We then have, from Eq. (3.30), that the estimate of spectral energy density is consistent with the limit of Eq. (3.27) for $\delta \rightarrow 1$

$$\Omega_{gw}(k, \tau) = \frac{r_T \mathcal{A}\mathcal{R} \Omega_{R0} c_3(\epsilon)}{12} \left(\frac{g_{\rho, r}}{g_{\rho, eq}} \right) \left(\frac{g_{s, eq}}{g_{s, r}} \right)^{4/3} \left(\frac{k}{a_1 H_1} \right)^{\bar{n}_T}, \quad \bar{n}_T \simeq -r_T/8, \quad (3.31)$$

both at the level of the amplitude and of the spectral index. Indeed from Eq. (3.25) we have that

$$\lim_{\delta \rightarrow 1, r_T \ll 1} n_T(\delta, r_T) = \lim_{r_T \ll 1} \left(2 - \frac{32}{16 - r_T} \right) \rightarrow -r_T/8, \quad (3.32)$$

and it coincides with \bar{n}_T appearing in Eq. (3.31). In this analysis a single post-inflationary stage between H_1 and H_r has been assumed but the obtained results can be easily generalized to the situation where a single phase is replaced by a series of different epochs⁶.

3.4 The maximal frequency

While deriving the explicit form of the spectral energy density we assumed throughout that $a_0 = 1$; this condition implies that at the present time comoving and physical wavenumbers coincide. Bearing in mind this point we can express more explicitly $k/(a_1 H_1)$:

$$\frac{k}{a_1 H_1} = \frac{k}{a_0 H_0} \left(\frac{a_0 H_0}{a_{eq} H_{eq}} \right) \left(\frac{a_{eq} H_{eq}}{a_r H_r} \right) \left(\frac{a_r H_r}{a_1 H_1} \right). \quad (3.33)$$

By now recalling that $k = 2\pi\nu$ we can therefore obtain the spectral energy density at the present time as a function of the comoving frequencies ν and ν_{max} since $x_1 = (\nu/\nu_{max})$. For instance, from Eq. (3.26) we have

$$\Omega_{gw}(\nu, \tau_0) = \frac{r_T \mathcal{A}\mathcal{R} \Omega_{R0} c_1(\epsilon)}{12 q^{2\delta}} \left(\frac{H_r}{H_1} \right)^{\alpha(\delta)} \left(\frac{g_{\rho, r}}{g_{\rho, eq}} \right) \left(\frac{g_{s, eq}}{g_{s, r}} \right)^{4/3} \left(\frac{\nu}{\nu_{max}} \right)^{n_T(\delta, r_T)}, \quad (3.34)$$

where the explicit value of the maximal frequency ν_{max} is now given by:

$$\nu_{max} = \frac{\sqrt{H_0 M_P}}{2\pi} (2\Omega_{R0})^{1/4} \sqrt{\frac{H_1}{M_P}} \left(\frac{g_{\rho, r}}{g_{\rho, eq}} \right)^{1/4} \left(\frac{g_{s, eq}}{g_{s, r}} \right)^{1/3} \left(\frac{H_r}{H_1} \right)^{\alpha(\delta)/4}. \quad (3.35)$$

The result of Eq. (3.35) can also be expressed, with shorthand notation, as $\nu_{max} = (H_r/H_1)^{\alpha(\delta)/4} \bar{\nu}_{max}$ where $\bar{\nu}_{max}$ corresponds to the maximal frequency when the post-inflationary evolution is dominated by radiation from H_1 down to H_{eq} . In this limit the explicit value of $\bar{\nu}_{max}$ falls in the range of $\mathcal{O}(300)$ MHz and, more precisely, we have

$$\bar{\nu}_{max} = 271.9 \left(\frac{h_0^2 \Omega_{R0}}{4.15 \times 10^{-5}} \right) \left(\frac{r_T}{0.06} \right)^{1/4} \left(\frac{\mathcal{A}\mathcal{R}}{2.41 \times 10^{-9}} \right)^{1/4} \left(\frac{g_{\rho, r}}{g_{\rho, eq}} \right)^{1/4} \left(\frac{g_{s, eq}}{g_{s, r}} \right)^{1/3} \text{ MHz}. \quad (3.36)$$

When $g_{s, r} = g_{\rho, r} = 106.75$ and $g_{s, eq} = g_{\rho, eq} = 3.94$ the evolution of the relativistic species suppresses $\bar{\nu}_{max}$ by a factor $\mathcal{O}(0.75)$; this means that $\bar{\nu}_{max}$ moves from 271.9 MHz down to 203.9 MHz. Both in Eqs. (3.31) and (3.35) we simply considered a single post-inflationary stage preceding the radiation-dominated evolution. The timeline of the expansion rate can be however more complicated and there may be different post-inflationary stages for curvature scales larger than H_r . In all these situations the bunch of frequencies $\nu = \mathcal{O}(\nu_{max})$ will always correspond to the wavelengths that left the horizon at the end of inflation and reentered immediately after. Depending on the timeline of the post-inflationary evolution there will however be other typical frequencies between below ν_{max} [46].

⁶The spectral energy density of Eq. (3.24) will then have more than one high frequency branch with different spectral indices characterizing each spectral domain. These possible extensions are not examined here but our results equally apply to a multi-stage post-inflationary evolution previously analyzed in Refs. [22, 23]

4 The transition matrix and the exact evaluation

If both $a(\tau)$ and $\mathcal{H}(\tau) = aH$ are continuous throughout all the stages of the dynamical evolution, at late times the mode functions and the spectral energy density can be computed from the elements of a transition matrix that relates the inflationary power spectra to their decelerated counterpart. From Eqs. (2.5) and (3.13) it follows that during the inflationary stage of expansion (see e.g. Eq. (3.14)) the explicit expressions of $f_k(\tau)$ and $g_k(\tau)$ are given by⁷ :

$$f_k(\tau) = \frac{N_\mu}{\sqrt{2k}} \sqrt{-k\tau} H_\mu^{(1)}(-k\tau), \quad \mu = \frac{3-\epsilon}{2(1-\epsilon)}, \quad (4.1)$$

$$g_k(\tau) = -N_\mu \sqrt{\frac{k}{2}} \sqrt{-k\tau} H_{\mu-1}^{(1)}(-k\tau), \quad (4.2)$$

where $N_\mu = \sqrt{\pi/2} e^{i\pi(2\mu+1)/4}$ while, as before, $\epsilon = -\dot{H}/H^2$; note that Eqs. (4.1)–(4.2) are valid for $\tau \leq -\tau_1$. Owing to the continuity of the background fields it is always possible to relate the mode functions for $\tau \geq -\tau_1$ to the ones defined during inflation and the general form of this relation depends on four coefficients that define the entries of the transition matrix:

$$f_k(\tau) = \mathcal{C}_{ff}(k, \tau, \tau_1) \bar{f}_k + \mathcal{C}_{fg}(k, \tau, \tau_1) \bar{g}_k/k, \quad (4.3)$$

$$g_k(\tau) = \mathcal{C}_{gf}(k, \tau, \tau_1) k \bar{f}_k + \mathcal{C}_{gg}(k, \tau, \tau_1) \bar{g}_k. \quad (4.4)$$

From Eqs. (4.1)–(4.2) we have that $\bar{f}_k = f_k(-\tau_1)$ and $\bar{g}_k = g_k(-\tau_1)$. The four functions \mathcal{C}_{ff} , \mathcal{C}_{fg} , \mathcal{C}_{gf} and \mathcal{C}_{gg} appearing in Eqs. (4.3)–(4.4) can be explicitly determined in all relevant situations where the continuity of the background fields is enforced. Furthermore, since the mode functions must always obey the Wronskian normalization condition of Eq. (2.8) the determinant of the transition matrix must be equal to 1

$$\mathcal{C}_{ff} \mathcal{C}_{gg} - \mathcal{C}_{fg} \mathcal{C}_{gf} = 1. \quad (4.5)$$

By construction the actual expressions of the coefficients $\mathcal{C}_{fg}(k, \tau, \tau_1)$ and $\mathcal{C}_{gf}(k, \tau, \tau_1)$ vanish in the limit $\tau \rightarrow -\tau_1$ so that

$$\begin{aligned} \lim_{\tau \rightarrow -\tau_1} \mathcal{C}_{ff}(k, \tau, \tau_1) &= \lim_{\tau \rightarrow -\tau_1} \mathcal{C}_{gg}(k, \tau, \tau_1) = 1, \\ \lim_{\tau \rightarrow -\tau_1} \mathcal{C}_{fg}(k, \tau, \tau_1) &= \lim_{\tau \rightarrow -\tau_1} \mathcal{C}_{gf}(k, \tau, \tau_1) = 0. \end{aligned} \quad (4.6)$$

The entries of the transition matrix depend on the conformal time coordinate τ , on the transition time-scale τ_1 and on the comoving wavenumber k . In our specific situation, given the form of Eqs. (4.3)–(4.4), it is convenient to introduce the dimensionless wavenumber $x_1 = k\tau_1$ and the shifted time variable $y \equiv y(\tau) = \tau + \tau_1(1+q)$ with the notable property that $y(-\tau_1) = q\tau_1$; we finally recall that $q = q(\epsilon, \delta) = (1-\epsilon)\delta$ has already been introduced in Eq. (3.14). We then have, by definition that the arguments of the entries of the transition matrix do not separately depend on k , τ_1 and τ but just on x_1 and ky ; so, for instance, $\mathcal{C}_{ff}(k, \tau, \tau_1) = \mathcal{C}_{ff}(x_1, ky)$ and similarly for all the other entries of the transition matrix. For technical reasons it is finally practical to present a separate treatment of the cases $\delta > 1/2$, $\delta \rightarrow 1/2$ and $0 < \delta < 1/2$.

4.1 Explicit form of the spectral energy density for $\delta > 1/2$

When $\delta > 1/2$ the Universe can expand either faster (i.e. $\delta > 1$) or slower (i.e. $1/2 < \delta < 1$) than radiation but in both regimes the elements of the transition matrix consist products of Bessel functions with indices

⁷As usual $H_\mu^{(1)}(z)$ denotes the Hankel function of first kind with index μ and argument z ; we also recall that, by definition, $H_\mu^{(2)}(z) = H_\mu^{(1)*}(z)$.

ν and $\nu + 1$ where, in this case, $\nu = \delta - 1/2 > 0$ [47, 48]. Their explicit form turns out to be:

$$\begin{aligned}
\mathcal{E}_{ff}(x_1, ky) &= \pi \sqrt{qx_1/2} \sqrt{ky/2} \left[J_{\nu+1}(qx_1) Y_\nu(ky) - Y_{\nu+1}(qx_1) J_\nu(ky) \right], \\
\mathcal{E}_{fg}(x_1, ky) &= \pi \sqrt{qx_1/2} \sqrt{ky/2} \left[J_\nu(qx_1) Y_\nu(ky) - Y_\nu(qx_1) J_\nu(ky) \right], \\
\mathcal{E}_{gf}(x_1, ky) &= \pi \sqrt{qx_1/2} \sqrt{ky/2} \left[Y_{\nu+1}(qx_1) J_{\nu+1}(ky) - J_{\nu+1}(qx_1) Y_{\nu+1}(ky) \right], \\
\mathcal{E}_{gg}(x_1, ky) &= \pi \sqrt{qx_1/2} \sqrt{ky/2} \left[Y_\nu(qx_1) J_{\nu+1}(ky) - Y_{\nu+1}(ky) J_\nu(qx_1) \right].
\end{aligned} \tag{4.7}$$

As expected from Eq. (4.6), for $\tau \rightarrow -\tau_1$ we have that⁸ $\mathcal{E}_{ff}(x_1, qx_1) = \mathcal{E}_{gg}(x_1, qx_1) = 1$; in the same limit, $\mathcal{E}_{fg}(x_1, qx_1) = \mathcal{E}_{gf}(x_1, qx_1) = 0$. If the post-inflationary evolution is dominated by a perfect irrotational fluid obeying all the energy conditions the maximal value of the barotropic index w corresponds to the minimal expansion rate, i.e. $\delta_{min} = 2/(3w_{max} + 1)$ and since w_{max} can be at most 1, $\delta_{min} \rightarrow 1/2$. The post-inflationary expansion rate may also correspond to a stage dominated by an oscillating scalar field [23]; in this case we can always approximate the potential as $(\varphi/\bar{M}_P)^{2q}$ near the origin [49] (see also [50, 51, 52]). In this situation the coherent oscillations lead to $\delta = (q + 1)/(2q - 1)$. For a quartic potential (i.e. $q \rightarrow 2$) we recover the case $\delta \rightarrow 1$ typical of a radiation phase while for $q \leq 2$ $\delta_{max} = 2$. The asymptote $\delta \rightarrow 1/2$ corresponds either to $q \gg 1$ or to the absence of the potential.

The spectral slopes and the amplitude of $\Omega_{gw}(k, \tau)$ will now be analyzed in all the relevant physical limits. From Eq. (2.14) the expression of the spectral energy density can first be expressed through the elements of the transition matrix⁹ given in Eq. (4.7)

$$\Omega_{gw}(k, \tau) = \frac{k^5}{6 H^2 \bar{M}_P^2 \pi^2 a^4} \left[\left| \mathcal{E}_{ff} \bar{f}_k + \mathcal{E}_{fg} \bar{g}_k/k \right|^2 + \left| \mathcal{E}_{gf} \bar{f}_k + \mathcal{E}_{gg} \bar{g}_k/k \right|^2 \right], \tag{4.8}$$

where, as already reminded in section 1, $\bar{M}_P = 1/\ell_P = M_P/\sqrt{8\pi}$. The two square moduli appearing in Eq. (4.8) equally contribute to the final result but the first term appearing in each square modulus dominates against the second. To clarify this hierarchy we can formally rewrite Eq. (4.8) as:

$$\Omega_{gw}(k, \tau) = \frac{k^5 |\bar{f}_k(x_1)|^2}{6 H^2 \bar{M}_P^2 \pi^2 a^4} \left[\mathcal{E}_{ff}^2 \left| 1 + \left(\frac{\mathcal{E}_{fg}}{\mathcal{E}_{ff}} \right) \left(\frac{\bar{g}_k}{k \bar{f}_k} \right) \right|^2 + \mathcal{E}_{gf}^2 \left| 1 + \left(\frac{\mathcal{E}_{gg}}{\mathcal{E}_{gf}} \right) \left(\frac{\bar{g}_k}{k \bar{f}_k} \right) \right|^2 \right], \tag{4.9}$$

where we used that the entries of the transition matrix are real while $\bar{f}_k(x_1)$ and $\bar{g}_k(x_1)$ are both complex. From Eqs. (4.3) and (4.4) $\bar{f}_k(x_1) = f_k(-\tau_1)$ and $\bar{g}_k(x_1) = g_k(-\tau_1)$ and their ratio only depends in x_1 which is always smaller than 1 as long as the frequencies are smaller than ν_{max} . For $x_1 > 1$ (i.e. $\nu > \nu_{max}$) the spectral energy density and the averaged multiplicity are exponentially suppressed [26, 27, 28, 29, 30] (see also [22, 23] and the forthcoming discussion of section 5). This means that, as long as $x_1 < 1$ (i.e. $k < a_1 H_1$), the momentum mode function \bar{g}_k is systematically smaller than $k \bar{f}_k$

$$\frac{\bar{g}_k(x_1)}{k \bar{f}_k(x_1)} = -\frac{H_{\mu-1}^{(1)}(x_1)}{H_\mu^{(1)}(x_1)} = -\frac{(1-\epsilon)x_1}{(1+\epsilon)} = -\frac{q(\epsilon, \delta)}{\delta} x_1 [1 - \epsilon + \mathcal{O}(\epsilon^2)], \tag{4.10}$$

while for $x_1 > 1$ the spectral energy density is suppressed because of the unitarity of the process of graviton production. Therefore, thanks to Eq. (4.10), both expressions appearing in the square moduli of Eq. (4.9)

⁸This result and result follows from Eq. (4.6) because of the explicit form of the Wronskian of Bessel functions [47, 48]. For $\tau \rightarrow -\tau_1$ we also have that $ky(-\tau_1) = qx_1$ so that, in this limit, all the arguments coincide.

⁹The arguments of all the various functions appearing in Eq. (4.8) have been omitted for the sake of conciseness but they will be reintroduced whenever needed.

are $\mathcal{O}(x_1^2)$ and therefore subleading when $x_1 < 1$ (i.e. $\nu < \nu_{max}$, see Eq. (3.33) and discussion therein). From a quantitative viewpoint in the case $\delta > 1/2$ we would have

$$\lim_{x_1 < 1} x_1 \frac{\mathcal{C}_{fg}(x_1, ky)}{\mathcal{C}_{ff}(x_1, ky)} = \lim_{x_1 < 1} x_1 \frac{\mathcal{C}_{gg}(x_1, ky)}{\mathcal{C}_{gf}(x_1, ky)} = \frac{(1 - \epsilon) \delta x_1^2}{(2\delta - 1)} \ll 1. \quad (4.11)$$

Equation (4.11) concretely demonstrates that the expansion scheme is not well defined for $\delta \rightarrow 1/2$ since the obtained results, in this limit, are formally divergent. This is why for $\delta \rightarrow 1/2$ there are logarithmic corrections that may affect the final expression of the spectral energy density; these issues are separately analyzed in the following subsection¹⁰.

The results of Eqs. (4.10) and (4.11) do not involve any assumption on $ky(\tau)$ and they hold for all the amplified wavelengths (i.e. $k < a_1 H_1$ and $\nu < \nu_{max}$) without further restrictions. The physical result we are after should however involve all the wavelengths that already reentered the Hubble radius (i.e. $ky(\tau) \simeq k\tau \gg 1$). Since the leading contribution to the spectral energy density of Eq. (4.9) follows from $\mathcal{C}_{ff}(x_1, ky)$ and $\mathcal{C}_{fg}(x_1, ky)$ we first write these entries in the limit $x_1 < 1$:

$$\begin{aligned} \mathcal{C}_{ff}(x_1, ky) &= (qx_1/2)^{-\delta} \sqrt{ky/2} J_{\delta-1/2}(ky) \Gamma(\delta + 1/2) [1 + \mathcal{O}(x_1)], \\ \mathcal{C}_{gf}(x_1, ky) &= -(qx_1/2)^{-\delta} \sqrt{ky/2} J_{\delta+1/2}(ky) \Gamma(\delta + 1/2) [1 + \mathcal{O}(x_1)]. \end{aligned} \quad (4.12)$$

When the results of Eq. (4.12) are combined with Eq. (4.9) the rapid oscillations get suppressed in the limit $ky > 1$ since $ky[J_{\delta-1/2}^2(ky) + J_{\delta+1/2}^2(ky)] \rightarrow 2/\pi$ as it follows from the large-argument limit of the Bessel functions [47, 48]. It is finally important to appreciate that the limits $x_1 < 1$ and $ky > 1$ commute and can be simultaneously enforced

$$\begin{aligned} &\left| \mathcal{C}_{ff}(x_1, ky) - \frac{H_{\mu-1}^{(1)}(x_1)}{H_{\mu}^{(1)}(x_1)} \mathcal{C}_{fg}(x_1, ky) \right|^2 + \left| \mathcal{C}_{gf}(x_1, ky) - \frac{H_{\mu-1}^{(1)}(x_1)}{H_{\mu}^{(1)}(x_1)} \mathcal{C}_{gg}(x_1, ky) \right|^2 \\ &= \frac{1}{\pi} (qx_1/2)^{-2\delta} \left[\Gamma^2(\delta + 1/2) + \mathcal{O}(x_1^2) + \mathcal{O}(|ky|^{-2}) \right]. \end{aligned} \quad (4.13)$$

Either from Eqs. (4.10)–(4.11) or from Eqs. (4.12)–(4.13) we can then deduce the spectral energy density of Eqs. (4.8)–(4.9) and obtain

$$\Omega_{gw}(k, \tau) = \bar{\Omega}(r_T, \delta, H_1, H_r) \left(\frac{k}{a_1 H_1} \right)^{n_T(\delta, r_T)} \left[1 + \mathcal{O}\left(\frac{k^2}{a_1^2 H_1^2} \right) \right]. \quad (4.14)$$

Equation (4.14) is valid when all the wavelengths of the spectrum are shorter than the Hubble radius; furthermore the value of $n_T(\delta, r_T)$ coincides exactly with the WKB result already obtained in Eq. (3.25). All the numerical factors entering $\Omega_{gw}(k, \tau)$ have been included inside the overall normalization $\bar{\Omega}(r_T, \delta, H_1, H_r)$

$$\bar{\Omega}(r_T, \delta, H_1, H_r) = \mathcal{B}(\delta, r_T) r_T \mathcal{A}_{\mathcal{R}} \Omega_{R0} \left(\frac{g_{\rho, r}}{g_{\rho, eq}} \right) \left(\frac{g_{s, eq}}{g_{s, r}} \right)^{4/3} \left(\frac{H_r}{H_1} \right)^{2(\delta-1)/(\delta+1)}. \quad (4.15)$$

The meanings of H_1 and H_r appearing in Eq. (4.15) coincide with the ones already introduced in the WKB analysis (see Eqs. (3.24)–(3.26) and discussions therein); as before the value of (H_1/M_P) follows from the amplitude to the scalar fluctuations of the geometry. Finally, in Eq. (4.15) the function $\mathcal{B}(\delta, r_T)$ is defined as:

$$\mathcal{B}(\delta, r_T) = \frac{2^{2(\mu+\delta)-3}}{3\pi^2 q^{2\delta}} \Gamma^2(\mu) \Gamma^2(\delta + 1/2), \quad \mu = \frac{48 - r_T}{32 - 2r_T}, \quad (4.16)$$

¹⁰For the moment we just remark that, provided $\delta > 1/2$ the contributions appearing in Eq. (4.9) can be analytically estimated with the negligible correction given in Eq. (4.11).

has been also introduced for convenience and it now contains the numerical factors that are essential for a comparison between the WKB approach and the present strategy. The largest value of $\mathcal{B}(\delta, r_T)$ corresponds to the limit $r_T \rightarrow 0$ where $\mathcal{B}(\delta, 0) = q^{-2\delta} \Gamma^2(\delta + 1/2)/(12\pi)$. In the limit $\delta \rightarrow 1$ the dependence on H_r fully disappear from Eq. (4.15) while $n_T(1, r_T) \rightarrow -r_T/8 + \mathcal{O}(r_T^2)$ which is the value of quasi-flat spectrum of the tensor modes when the consistency relations are enforced.

4.2 The case $\delta \rightarrow 1/2$ and its spectral features

As already mentioned in Eq. (4.11) the concurrent expansions in terms of x_1 and ky are not well defined when $\delta \rightarrow 1/2$. In this physical case the expansion rate is slower than radiation and the entries of the transition matrix are:

$$\begin{aligned}\mathcal{E}_{ff}(x_1, ky) &= \pi\sqrt{qx_1/2}\sqrt{ky/2}\left[J_1(qx_1)Y_0(ky) - Y_1(qx_1)J_0(ky)\right], \\ \mathcal{E}_{fg}(x_1, ky) &= \pi\sqrt{qx_1/2}\sqrt{ky/2}\left[J_0(qx_1)Y_0(ky) - Y_0(qx_1)J_0(ky)\right], \\ \mathcal{E}_{gf}(x_1, ky) &= \pi\sqrt{qx_1/2}\sqrt{ky/2}\left[Y_1(qx_1)J_1(ky) - J_1(qx_1)Y_1(ky)\right], \\ \mathcal{E}_{gg}(x_1, ky) &= \pi\sqrt{qx_1/2}\sqrt{ky/2}\left[Y_0(qx_1)J_1(ky) - Y_1(ky)J_0(qx_1)\right].\end{aligned}\quad (4.17)$$

The results of Eq. (4.17) may also follows from Eq. (4.25) by recalling that, in general terms, $Y_{-1}(z) = -Y_1(z)$ and $J_{-1}(z) = -J_1(z)$. We know that the small argument limit of $Y_0(z)$ is logarithmically divergent [47, 48]; as suggested long ago and this is the reason why a series of logarithmic corrections must be included in the expression of the transfer function [30]. This is why Eq. (4.17) already suggests the reason of the logarithmic divergences potentially appearing in the expansion of Eq. (4.11) for $\delta \rightarrow 1/2$. In the limit $\delta \rightarrow 1/2$ we have that $q(\delta, \epsilon) = \delta(1 - \epsilon) \simeq 1/2$ and if we expand the spectral energy density for $qx_1 \ll 1$ the partial results for the two contributions appearing in the spectral energy density become:

$$\begin{aligned}\mathcal{E}_{ff}(x_1, ky) - x_1\mathcal{E}_{fg}(x_1, ky) &= \frac{ky}{qx_1}J_0^2(ky) + (ky/2)J_0(ky)\left\{J_0(ky)\left[1 + 6\gamma + 6\ln(qx_1/2)\right] - 3\pi Y_0(ky)\right\}qx_1 + \mathcal{O}(q^3x_1^3), \\ \mathcal{E}_{gf}(x_1, ky) - x_1\mathcal{E}_{gg}(x_1, ky) &= \frac{ky}{qx_1}J_1^2(ky) + (ky/2)J_1(ky)\left\{J_1(ky)\left[1 + 6\gamma + 6\ln(qx_1/2)\right] - 3\pi Y_1(ky)\right\}qx_1 + \mathcal{O}(q^3x_1^3).\end{aligned}\quad (4.18)$$

where $\gamma = 0.5772$ is the Euler-Mascheroni constant. We can then compute explicitly the contribution to the spectral energy density

$$\begin{aligned}&\left|\mathcal{E}_{ff}(x_1, ky) - x_1\mathcal{E}_{fg}(x_1, ky)\right|^2 + \left|\mathcal{E}_{gf}(x_1, ky) - x_1\mathcal{E}_{gg}(x_1, ky)\right|^2 = \\ &\frac{ky}{qx_1}\left[J_0^2(ky) + J_1^2(ky)\right] + qx_1(ky/2)\left\{-3\pi\left[J_0(ky)Y_0(ky) + J_1(ky)Y_1(ky)\right] + \left[J_0^2(ky) + J_1^2(ky)\right]\left[1 + 6\gamma - 6\ln(qx_1/2)\right]\right\}.\end{aligned}\quad (4.19)$$

Again the terms containing the combinations of the type $J_0^2(z)$ and of $J_1^2(z)$ have a well defined large-argument limit which is of the order of $2/(\pi z)$; this is also the case for the combination $Y_0^2(z) + Y_1^2(z) \rightarrow 2/(\pi z)$ for $z \gg 1$. The mixed combinations of the type $J_0(z)Y_0(z) + J_1(z)Y_1(z)$ oscillate around 0 in the

limit $z \gg 1$ and are subleading the perturbative expansion. For this reason the right-hand side of Eq. (4.19) simply becomes:

$$\frac{2}{\pi q x_1} + \frac{q x_1}{\pi} \left[1 + 6\gamma - 6 \ln(q x_1/2) \right]. \quad (4.20)$$

The same strategy leading to Eq. (4.20) can be enforced order by order; for instance the following correction to Eq. (4.20) reads:

$$\frac{q^3 x_1^3}{16\pi} \left\{ \begin{aligned} & 18\pi^2 + 29 + 4 \ln 2 + 72(\gamma^2 + \ln^2 2) - 4\gamma(1 + 36 \ln 2) \\ & + 4 \ln(q x_1) \left[-1 + 36\gamma + 18 \ln(q x_1) - 36 \ln 2 \right] \end{aligned} \right\}. \quad (4.21)$$

As a final step we can therefore deduce the expression of the spectral energy density valid for $\delta \rightarrow 1/2$ and in the limit where all the wavelengths of the spectrum are shorter than the Hubble radius:

$$\Omega_{gw}(k, \tau) = \frac{4}{3\pi^2 q} \left(\frac{H_1}{M_P} \right)^2 \left(\frac{H_1^2 a_1^4}{H^2 a^4} \right) \left(\frac{k}{a_1 H_1} \right)^{m_T(r_T)} \left[1 + q^2 x_1^2 \ell_1(x_1) + q^3 x_1^3 \ell_2(x_1) + \mathcal{O}(q^5 x_1^5) \right], \quad (4.22)$$

where the higher order terms of the expansion also contain the same kind of logarithmic corrections appearing in the two functions $\ell_1(x_1)$ and $\ell_2(x_1)$

$$\begin{aligned} \ell_1(x_1) &= \frac{1}{2} \left[1 + 6\gamma + 6 \ln(q x_1/2) \right], \\ \ell_2(x_1) &= \frac{1}{32} \left[18\pi^2 + 4 \ln 2 + (72\gamma^2 - 4\gamma + 29) \right. \\ &\quad \left. + 144(\gamma - \ln 2 - 1) \ln(q x_1/2) + 72 \ln^2(q x_1/2) \right]. \end{aligned} \quad (4.23)$$

In Eq. (4.22) the spectral index $m_T(r_T)$ coincides with $n_T(\delta, r_T)$ introduced in Eq. (4.14) in the limit $\delta \rightarrow 1/2$:

$$m_T(r_T) = \lim_{\delta \rightarrow 1/2} n_T(\delta, r_T) = \frac{16 - 3 r_T}{16 - r_T}. \quad (4.24)$$

4.3 The transition matrix for $0 < \delta < 1/2$

The last case we are going to discuss involves the range $0 < \delta < 1/2$; also in this situation the expansion rate is always slower than radiation and the explicit form of the transition matrix is:

$$\begin{aligned} \mathcal{E}_{ff}(x_1, ky) &= \pi \sqrt{q x_1/2} \sqrt{k y/2} \left[Y_{\nu-1}(q x_1) J_\nu(ky) - J_{\nu-1}(q x_1) Y_\nu(ky) \right], \\ \mathcal{E}_{fg}(x_1, ky) &= \pi \sqrt{q x_1/2} \sqrt{k y/2} \left[J_\nu(q x_1) Y_\nu(ky) - Y_\nu(q x_1) J_\nu(ky) \right], \\ \mathcal{E}_{gf}(x_1, ky) &= \pi \sqrt{q x_1/2} \sqrt{k y/2} \left[Y_{\nu-1}(q x_1) J_{\nu-1}(ky) - J_{\nu-1}(q x_1) Y_{\nu-1}(ky) \right], \\ \mathcal{E}_{gg}(x_1, ky) &= \pi \sqrt{q x_1/2} \sqrt{k y/2} \left[J_\nu(q x_1) Y_{\nu-1}(ky) - J_{\nu-1}(ky) Y_\nu(q x_1) \right], \end{aligned} \quad (4.25)$$

with the further difference that in Eq. (4.25) $\nu = 1/2 - \delta > 0$. In spite of the differences between Eqs. (4.25) and (4.7) the spectral energy density in critical units ultimately coincide in the two cases. To verify this result we can use the conclusions of the previous analysis implying that two physical limits $x_1 < 1$ and

$ky > 1$ commute; we can therefore expand the result of Eq. (4.25) and the result is:

$$\begin{aligned}
\mathcal{E}_{ff}(x_1, y) &= -(qx_1/2)^{-\delta} \left\{ \frac{\Gamma(\delta + 1/2)}{\sqrt{\pi}} \cos[\pi(\delta + 1/2)] \cos[ky + \pi(\delta - 1)/2] \right. \\
&\quad \left. + \frac{\sqrt{\pi}}{\Gamma(1/2 - \delta)} \sin[ky + \pi(\delta - 1)/2] + \mathcal{O}(x_1) + \mathcal{O}(|ky|^{-2}) \right\}, \\
\mathcal{E}_{fg}(k, x_1, y) &= (qx_1/2)^\delta \left\{ \frac{\Gamma(1/2 - \delta)}{\sqrt{\pi}} \cos[ky + \pi(\delta - 1)/2] + \mathcal{O}(x_1) + \mathcal{O}(|ky|^{-2}) \right\}, \\
\mathcal{E}_{gf}(k, x_1, y) &= -(qx_1/2)^{-\delta} \left\{ \frac{\Gamma(\delta + 1/2)}{\sqrt{\pi}} \cos[\pi(\delta + 1/2)] \cos[ky + \pi\delta/2] \right. \\
&\quad \left. + \frac{\sqrt{\pi}}{\Gamma(1/2 - \delta)} \sin[ky + \pi\delta/2] + \mathcal{O}(x_1) + \mathcal{O}(|ky|^{-2}) \right\}, \\
\mathcal{E}_{gg}(k, x_1, y) &= (qx_1/2)^\delta \left\{ \frac{\Gamma(1/2 - \delta)}{\sqrt{\pi}} \cos[ky + \pi\delta/2] + \mathcal{O}(x_1) + \mathcal{O}(|ky|^{-2}) \right\}. \tag{4.26}
\end{aligned}$$

From Eq. (4.26) we can verify the validity of all the approximations employed so far. This means that to leading order in (qx_1) and $|ky|^{-2}$ the spectral energy in critical units can also be written as

$$\Omega_{gw}(k, \tau) = \frac{k^5 |\bar{f}_k(x_1)|^2}{6 H^2 \bar{M}_P^2 \pi^2 a^4} \left[\mathcal{E}_{ff}^2(k, x_1, y) + \mathcal{E}_{gf}^2(k, x_1, y) + \mathcal{O}(x_1^2) \right]. \tag{4.27}$$

If Eq. (4.26) is now inserted into Eq. (4.27) the spectral energy density in critical units becomes:

$$\Omega_{gw}(k, \tau) = \bar{\Omega}(r_T, \delta, H_1, H_r) \left(\frac{k}{a_1 H_1} \right)^{n_T(\delta, r_T)} \left[1 + \mathcal{O}\left(\frac{k^2}{a_1^2 H_1^2} \right) \right], \tag{4.28}$$

which coincides exactly with the result of Eq. (4.14) except for the explicit form of $\mathcal{B}(\delta, r_T)$ that now reads:

$$\mathcal{B}(\delta, r_T) = \frac{2^{2\mu-3}}{3 \pi^2 q^{2\delta}} \Gamma^2(\mu) \Gamma^2(\delta + 1/2) \left\{ \cos^2[\pi(\delta + 1/2)] + \frac{\pi^2}{\Gamma^2(1/2 - \delta) \Gamma^2(1/2 + \delta)} \right\}, \tag{4.29}$$

where, as before, $\mu = (48 - r_T)/(16 - r_T)$. While Eqs. (4.16) and (4.29) seem superficially different but they lead to the same condition¹¹. Although the results of Eqs. (4.14) and (4.27) are formally the same they apply for two different ranges of δ , i.e. $\delta > 1/2$ and $0 \leq \delta < 1/2$ respectively.

4.4 Comparison of the different strategies

The spectral energy densities in critical units determined from the WKB approximation and from the transition matrix are overall consistent and the mismatch between the two complementary approaches can be unambiguously quantified. This analysis is useful since the analytic determinations can be reasonably employed in order to normalize the high frequency branch of the spectrum. Let us first consider the case where $\delta \neq 1/2$ and denote by $\mathcal{D}(\delta, r_T)$ the ratio between the WKB estimate (see Eqs. (3.27) and (3.34)) and the result based on the transition matrix (see Eqs. (4.14) and (4.28)):

$$\mathcal{D}(\delta, r_T) = \frac{c_1(r_T/16)}{12 \mathcal{B}(\delta, r_T) q^{2\delta}}. \tag{4.30}$$

¹¹Because of the usual identities involving the Gamma functions we have that $\pi \sin \pi\delta = \Gamma(1/2 - \delta) \Gamma(1/2 + \delta)$; this observation implies immediately that the quantity within the squared brackets is just 1.

With simple algebra involving the explicit form of $\mathcal{B}(\delta, r_T)$ (see, for instance, Eq. (4.16)) Eq. (4.30) becomes

$$\mathcal{D}(\delta, r_T) = \frac{4\pi^2[1024 + (16 - r_T)^2]}{2^{2\delta+(48-r_T)/(16-r_T)}(48 - r_T)^2 \Gamma^2(\delta + 1/2) \Gamma^2[(48 - r_T)/(32 - r_T)]}. \quad (4.31)$$

To appreciate the numerical relevance of the mismatch between the two approaches we can consider the limit of Eq. (4.31) $r_T \rightarrow 0$ and obtain:

$$\lim_{r_T \rightarrow 0} \mathcal{D}(\delta, r_T) = \frac{10\pi}{9} \frac{2^{-2\delta}}{\Gamma^2(\delta + 1/2)}. \quad (4.32)$$

Equations (4.31) and (4.32) show that the WKB approximation always underestimates the spectral energy density for very large values of δ but it is consistent with the exact result within a factor of 10 for $\delta < 3$. In the case $\delta \rightarrow 1/2$ the logarithmic corrections obtained within the WKB approach follow from Eqs. (3.18) and (3.19). The comparison with Eqs. (4.22)–(4.23) demonstrates that the structure of the logarithmic corrections is different within the two approaches. The approximations can be also compared with the results based on the exact form

5 The accuracy of high frequency normalization

The approximations discussed in the previous sections are mutually consistent and they can be used to assess various properties of the high frequency signal without preliminary knowledge of the spectrum at lower frequencies. While this procedure inevitably contains some inaccuracies that are quantified hereunder, the semi-analytic approach is often swifter than the full numerical analysis. Within this logic the first point will now be to scrutinize (both exactly and approximately) the averaged multiplicity of the produced pairs and its exponential suppression. After clarifying the scaling properties of the averaged multiplicity the same analysis shall be extended to the spectral energy density. In the second part of this section we are going to compare the high and low frequency normalizations imposed, respectively, on the analytic spectrum (that disregards the low frequency region) and on the numerical results (that take also into account the late-time sources of suppression in the nHz region). The bounds on the post-inflationary expansion history and the expected ranges of the chirp amplitudes are finally analyzed in the last part of the section. We are going to argue that for a direct detection of a cosmic signal in the ultra-high frequency band the required chirp amplitudes should be at least twelve orders of magnitude smaller than the ones currently measured in the audio band ranging between few Hz and ten kHz.

5.1 Scaling of the averaged multiplicity and the single-graviton limit

The approximation schemes of sections 3 and 4 are based on the enforcement of the two concurrent limits namely $x_1 < 1$ and $ky > 1$. While both requirements are physically justified the former is more general than the latter insofar as it is always accurately verified below the maximal frequency domain (i.e. $\nu < \nu_{max}$). The averaged multiplicity is the appropriate dimensionless variable that encodes the relevant information on the production of the pairs of gravitons and this is why it is practical to study it both exactly and approximately. In a quantum mechanical perspective, the amplification of the mode functions corresponds to the production of graviton pairs with opposite three-momenta. Indeed, from the explicit form of the quantum Hamiltonian we have [23]:

$$\hat{H}_g(\tau) = \frac{1}{2} \int d^3k \sum_{\alpha=\oplus, \otimes} \left\{ k \left[\hat{a}_{\vec{k}, \alpha}^\dagger \hat{a}_{\vec{k}, \alpha} + \hat{a}_{-\vec{k}, \alpha} \hat{a}_{-\vec{k}, \alpha}^\dagger \right] + \lambda \hat{a}_{-\vec{k}, \alpha}^\dagger \hat{a}_{\vec{k}, \alpha}^\dagger + \lambda^* \hat{a}_{\vec{k}, \alpha} \hat{a}_{-\vec{k}, \alpha} \right\}, \quad (5.1)$$

where $\lambda = i\mathcal{H} = iaH$. The three classes of terms quadratic in the creation and annihilation operators are in fact the generators of the $SU(1, 1)$ group and the evolution equations for $\hat{a}_{\vec{k}}^\dagger$ and $\hat{a}_{-\vec{k}, \alpha}^\dagger$ in the Heisenberg

description follow from the Hamiltonian (5.1):

$$\begin{aligned}\frac{d\widehat{a}_{\vec{k},\alpha}^-}{d\tau} &= i[\widehat{H}_g, \widehat{a}_{\vec{k},\alpha}^-] = -ik\widehat{a}_{\vec{k},\alpha}^- - i\lambda\widehat{a}_{-\vec{k},\alpha}^\dagger, \\ \frac{d\widehat{a}_{-\vec{k},\alpha}^\dagger}{d\tau} &= i[\widehat{H}_g, \widehat{a}_{-\vec{k},\alpha}^\dagger] = ik\widehat{a}_{-\vec{k},\alpha}^\dagger + i\lambda^*\widehat{a}_{\vec{k},\alpha}^-.\end{aligned}\quad (5.2)$$

The explicit evolution of the creation and annihilation operators given by Eq. (5.2) can be solved by introducing two (complex) functions $u_{k,\alpha}(\tau)$ and $v_{k,\alpha}(\tau)$:

$$\begin{aligned}\widehat{a}_{\vec{k},\alpha}^-(\tau) &= u_{k,\alpha}(\tau)\widehat{b}_{\vec{k},\alpha}^- - v_{k,\alpha}(\tau)\widehat{b}_{-\vec{k},\alpha}^\dagger, \\ \widehat{a}_{-\vec{k},\alpha}^\dagger(\tau) &= u_{k,\alpha}^*(\tau)\widehat{b}_{-\vec{k},\alpha}^\dagger - v_{k,\alpha}^*(\tau)\widehat{b}_{\vec{k},\alpha}^-.\end{aligned}\quad (5.3)$$

The complex functions $u_k(\tau)$ and $v_k(\tau)$ can be directly related to the mode functions defined earlier on $f_k(\tau) = [u_k(\tau) - v_k^*(\tau)]/\sqrt{2k}$ and as $g_k(\tau) = -i\sqrt{k/2}[u_k(\tau) + v_k^*(\tau)]$. Because of the unitarity of the evolution the two complex functions are subjected to the constraint $|u_{k,\alpha}(\tau)|^2 - |v_{k,\alpha}(\tau)|^2 = 1$; the averaged multiplicity of the produced gravitons with opposite three-momenta follows from Eq. (5.3) and it is given by

$$\langle \widehat{N}_k(\tau) \rangle = \sum_{\alpha=\oplus,\otimes} \left[\langle \widehat{N}_{\vec{k},\alpha}^-(\tau) \rangle + \langle \widehat{N}_{-\vec{k},\alpha}^\dagger(\tau) \rangle \right] = 4|v_k(\tau)|^2. \quad (5.4)$$

The factor 4 counts the gravitons with opposite three-momenta summed over the two polarizations and this means that in Eq. (5.4) $\bar{n}(k, \tau) = |v_k(\tau)|^2$ denotes the multiplicity of the pairs associated with a single tensor polarization. Thus the averaged multiplicity depends on the elements of the transition matrix and solely depends on the dimensionless variables x_1 and ky :

$$\begin{aligned}\bar{n}(x_1, ky) &= \frac{\pi x_1}{8} \left\{ \left[\mathcal{E}_{ff}^2(x_1, ky) + \mathcal{E}_{gg}^2(x_1, ky) \right] \left[J_\mu^2(x_1) + Y_\mu^2(x_1) \right] \right. \\ &\quad + \left[\mathcal{E}_{fg}^2(x_1, ky) + \mathcal{E}_{gf}^2(x_1, ky) \right] \left[J_{\mu-1}^2(x_1) + Y_{\mu-1}^2(x_1) \right] \\ &\quad \left. - 2 \left[\mathcal{E}_{ff}(x_1, ky) \mathcal{E}_{fg}(x_1, ky) + \mathcal{E}_{gf}(x_1, ky) \mathcal{E}_{gg}(x_1, ky) \right] \right\}.\end{aligned}\quad (5.5)$$

We stress that the averaged multiplicity counts in fact the produced gravitons in spite of the vacuum contribution which can be always renormalized [10, 22, 23] but this is immaterial when the averaged multiplicities are very large. In the limit $ky \gg 1$ and x_1 the averaged multiplicities are estimated for the different values of the parameters with the same approximation schemes analyzed in section 4; from Eq. (5.5) we consider, in particular, the limit $ky \gg 1$ and deduce the momentum (or frequency) dependence of the averaged multiplicity

$$\bar{n}(x_1) = \lim_{x_1 < 1, ky \gg 1} \bar{n}(x_1, ky) = 3\mathcal{B}(\delta, r_T) x_1^{n_T(\delta, r_T) - 4}, \quad (5.6)$$

where $\mathcal{B}(\delta, r_T)$ has been already introduced in Eq. (4.16) while $n_T(\delta, r_T)$ follows from Eq. (3.25). The analytic results of Eq. (5.6) are illustrated by the full line in both plots of Fig. 1. For a selection of parameters the analytic approximation is compared with the exact result of Eq. (5.5) where $ky_0 = ky(\tau_0) = 10^{18}$. It can be checked that different typical values of ky_0 lead exactly to the same result as long as $ky_0 \gg 1$. The results of Fig. 1 clarify the interplay between the analytic approximations and the scaling properties of the average multiplicity. The estimates based on Eq. (5.6) differ from the exact results by factors that are $\mathcal{O}(10^{-2})$, as it is apparent from the scale of variation of $\bar{n}(x_1)$ in both plots of Fig. 1. In the limit $\delta \rightarrow 1$ the result of Eq. (5.6) reproduces the averaged multiplicity of the concordance scenario where

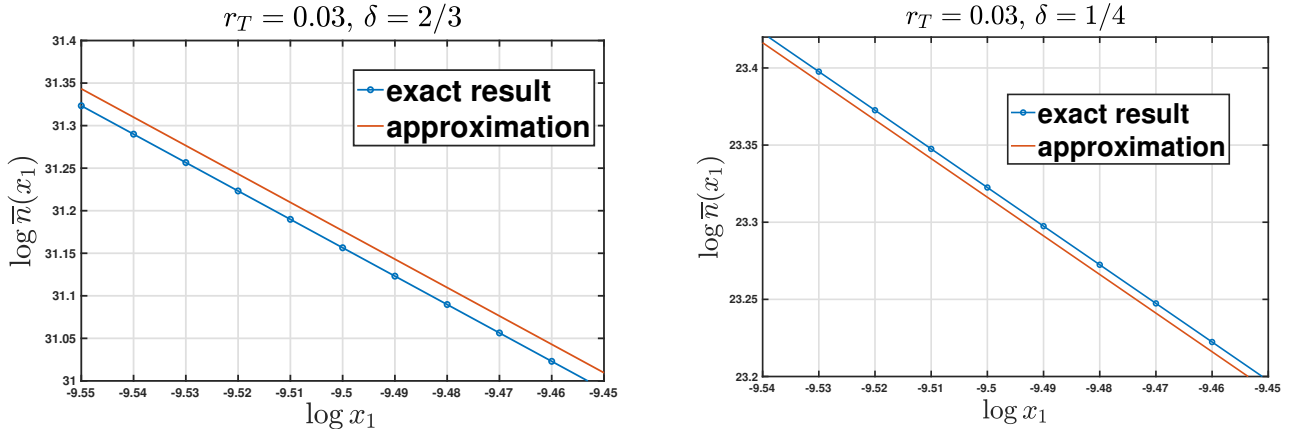


Figure 1: We compare the exact results based on Eq. (5.5) with the approximations leading to Eq. (5.6). Common logarithms are employed on both axes. The highly restricted range of variation of x_1 clarifies better than any other consideration the accuracy of the analytic approximation discussed in section 5.

an inflationary stage is replaced by an evolution dominated by radiation; in this case $n_T \rightarrow -r_T/8$ and $\bar{n}(x_1) \propto x_1^{-4-r_T/8}$. In this last case the spectral energy density is therefore (approximately) scale-invariant and the average multiplicity is strongly non-thermal.

Since the dimensionless variable x_1 is related to the ratio between ν and ν_{max} , as the frequency scale increases there will necessarily be a region where $\bar{n}(\nu, \tau_0) \rightarrow \mathcal{O}(1)$ and this is, from the operational viewpoint, the maximal frequency range of the spectrum. There are in fact two complementary ways in which ν_{max} can be determined [22]. As established from Eqs. (3.35)–(3.36)) ν_{max} follows indirectly from the expansion rate after inflation and from the minimal value of the Hubble radius at the end of the inflationary stage. Conversely, in a quantum mechanical perspective, the maximal frequency of the spectrum corresponds to the production of few pairs of gravitons with opposite comoving three-momenta before the averaged multiplicity is exponentially suppressed

$$\lim_{x_1 \rightarrow 1} \bar{n}(x_1) = \mathcal{O}(1), \quad \nu \rightarrow \nu_{max}. \quad (5.7)$$

Indeed, while the averaged multiplicity for $x_1 < 1$ (i.e. $\nu < \nu_{max}$) corresponds to the mean number of produced pairs for $x_1 > 1$ the averaged multiplicity is suppressed exponentially or, more precisely [24, 25, 26],

$$\frac{|\bar{n}(x_1)|^2}{1 + |\bar{n}(x_1)|^2} = e^{-\gamma x_1}, \quad x_1 > 1. \quad (5.8)$$

The degree of suppression of Eq. (5.8) depends on γ , i.e. a numerical factor $\mathcal{O}(1)$ controlled by the smoothness of the transition between the inflationary and the post-inflationary phase; the value of γ can be numerically estimated if the evolution of the mode functions is carefully integrated frequency by frequency [30]. By looking simultaneously at Eqs. (5.6) and (5.8) the averaged multiplicity of pairs produced from the vacuum can be written in the following suggestive form:

$$\bar{n}(x_1) = \frac{3\gamma \mathcal{B}(\delta, r_T) x_1^{n_T-3}}{e^{\gamma x_1} - 1}, \quad x = (\nu/\nu_{max}). \quad (5.9)$$

Equation (5.9) interpolates between the power-law behaviour of Eq. (5.6) and the exponential suppression of Eq. (5.8). This means that the spectrum of relic gravitons is in fact a distorted thermal spectrum as argued long ago [54]; this conclusion is incidentally consistent with the multiplicity distribution of the relic gravitons which is of Bose-Einstein type [22]. The exact result of Eq. (5.5) is illustrated in Fig. 2

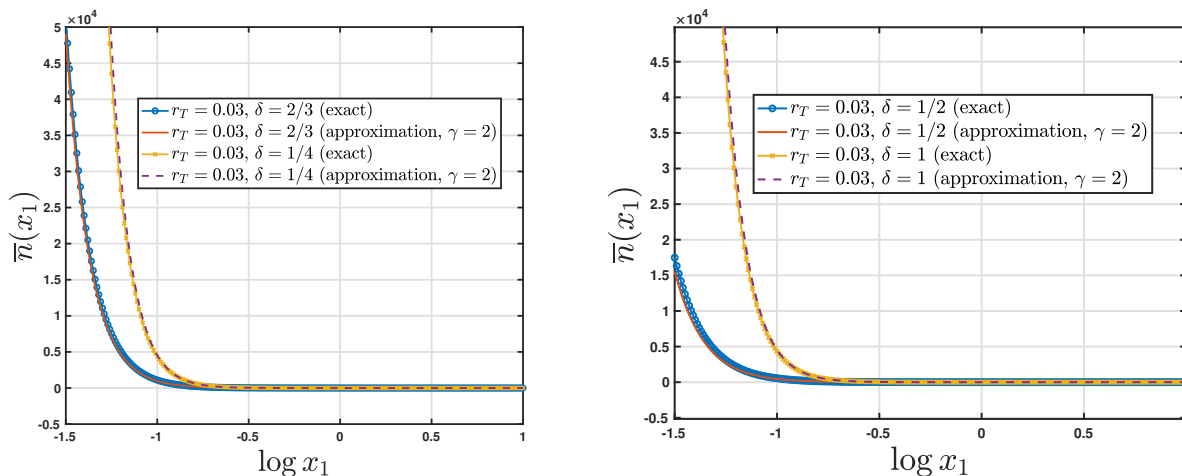


Figure 2: In both plots we compare the exact results based on Eq. (5.5) with the approximations discussed in Eq. (5.9). Unlike the case of Fig. 1, to ease the comparison and to clarify the exponential suppression, the average multiplicity has been illustrated on a linear scale as a function of the common logarithm of x_1 . We can also appreciate from both plots that when $\gamma \rightarrow 2$ the exact result is well represented by the analytic approximation.

and compared with the interpolation of Eqs. (5.8)–(5.9). We selected the same value of $k y_0$ employed in Fig. 1; as previously remarked, as long as limit $k y_0 \gg 1$ the specific value is immaterial. In Fig. 2 we considered the range around the maximal frequency corresponding to $x_1 = \mathcal{O}(1)$ and from the comparison illustrated in Fig. 2 we can infer that Eq. (5.9) reproduces the exact results for $\gamma = \mathcal{O}(2)$. It is known that the specific amount of exponential suppression depends on the nature of the transition regime that has been numerically discussed in Refs. [30]. It is however interesting that the minimal framework leading to Eq. (5.5) (based on the continuity of the transition matrix and of the background) generally suggests $\gamma = \mathcal{O}(2)$. As we are going to see in a moment, the exponential suppression for $\nu > \nu_{max}$ also guarantees the convergence of the integrated spectral energy density over the whole frequency domain [30] (see also [22]).

5.2 Scaling of the spectral energy density

The averaged multiplicity $\bar{n}(x_1, k y)$ can be related to the rescaled spectral energy density in critical units denoted hereunder by $\omega_{gw}(x_1, k y)$:

$$\omega_{gw}(x_1, k y) = x_1^4 \bar{n}(x_1, k y). \quad (5.10)$$

This analysis is useful for numerical purposes but $\omega_{gw}(x_1, k y)$ is simply related to the value of $\Omega_{gw}(x_1, k y)$; more specifically the relation between the two parametrizations does not depend on the frequency and it is given by:

$$\Omega_{gw}(x_1, k y) = \frac{8}{3\pi} \left(\frac{H_1}{M_P} \right)^2 \left(\frac{H_1^2 a_1^4}{H^2 a^4} \right) \omega_{gw}(x_1, k y). \quad (5.11)$$

It follows from the result of Eq. (5.6) that $\omega_{gw}(x_1, k y)$ should scale as

$$\lim_{x_1 < 1, k y \gg 1} \frac{\omega_{gw}(x_1, k y)}{x_1^{n_T}} = 3 \mathcal{B}(\delta, r_T), \quad (5.12)$$

so that the ratio $\omega_{gw}(x_1, k y)/x_1^{n_T}$ does not depend on x_1 but only on the specific values of r_T and δ encoded in the expression of $\mathcal{B}(\delta, r_T)$. In Fig. 3 we illustrate the common logarithm of the ratio $\omega_{gw}(x_1, k y)/x_1^{n_T}$

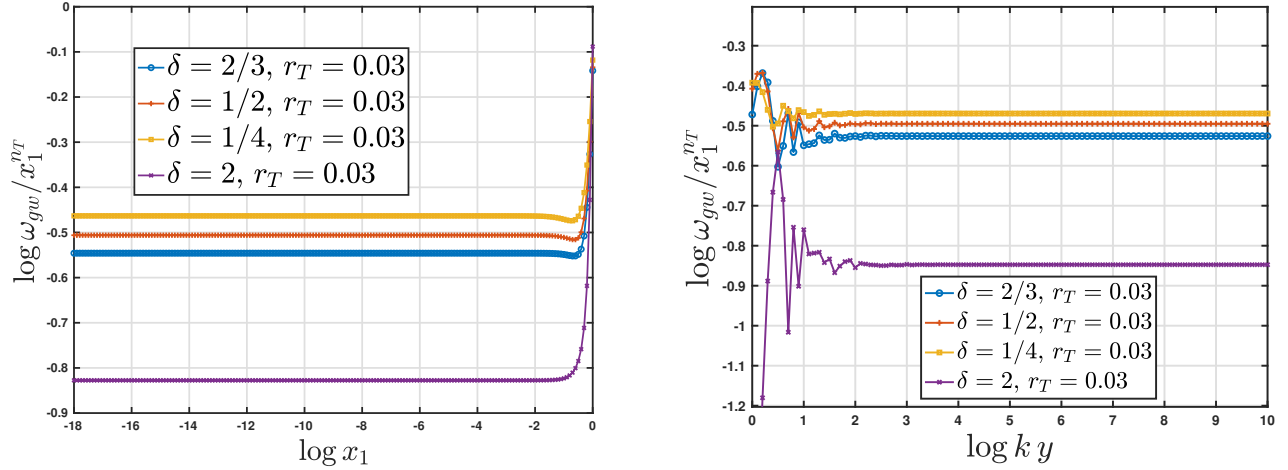


Figure 3: In the left plot the common logarithm of $\omega_{gw}(x_1, ky)/x_1^{n_T}$ is illustrated as a function of the common logarithm of x_1 when $r_T = 0.03$ and for different values of δ . Although the value of ky is immaterial (as long as $ky > 1$) the left plot has been obtained for $ky = 10^{15}$. In the right plot the value of x_1 has been fixed to 10^{-8} and the common logarithm of $\omega_{gw}(x_1, ky)/x_1^{n_T}$ has been illustrated as a function of the common logarithm of ky .

as a function of the common logarithm of x_1 . As expected from Eq. (5.12) the results of Fig. 2 are scale-invariant and the explicit values of the plateau are correctly estimated by the analytic approximation with the same accuracy illustrated by Fig. 1. This means that the analytic expressions of the spectral energy density in critical units can be used to infer the chirp amplitudes and the potential signals in different frequency ranges.

The present analysis suggests that the high frequency and ultra-high frequency signals can be estimated according to a twofold strategy. In the first approach the potential signal is normalized well below the maximal frequency whereas, in the second possibility, the spectral energy density is directly fixed at the maximal frequency; this twofold strategy is illustrated in Fig. 4. In the realistic situation the analytic approximation discussed so far only makes sense for sufficiently large frequencies

$$\nu > \nu_r = \frac{(2\Omega_{R0})^{1/4}}{2\pi} \sqrt{H_0 H_r} \left(\frac{g_{\rho,r}}{g_{\rho,eq}} \right)^{1/4} \left(\frac{g_{s,eq}}{g_{s,r}} \right)^{1/3}, \quad (5.13)$$

where H_r now denotes the value of the expansion rate at the onset of the radiation-dominated stage. From Eq. (5.13) the explicit value of ν_r is related to $\bar{\nu}_{max}$ since, by definition, $\nu_r/\bar{\nu}_{max} = \sqrt{H_r/H_1}$. One possibility is therefore to normalize the spectral energy density in critical units for $\nu \rightarrow \nu_r$, as illustrated in the left plot of Fig. 4. A complementary strategy is to match $h_0^2 \Omega_{gw}(\nu, \tau_0)$ with its maximally allowed value at the frequency of the spike, as suggested in the right plot of Fig. 4. In this case, however, the maximum of the spectral energy density should be determined in absolute terms [22]. In Fig. 4 we have set this absolute value to be $\mathcal{O}(0.1)$ THz.

It is appropriate to mention, at this point, that the timeline of the expansion rate can be more complicated than the one considered so far. In this case all the considerations discussed here in the case of a single post-inflationary stage can be extended exactly with the same techniques by following the considerations developed, at length, in Ref. [46]. Depending on the number of the intermediate stages also the typical frequencies of the spectrum increase. Rather than starting from the general considerations it is better to consider a specific example. For instance in the case of two successive intermediate phases with expansion

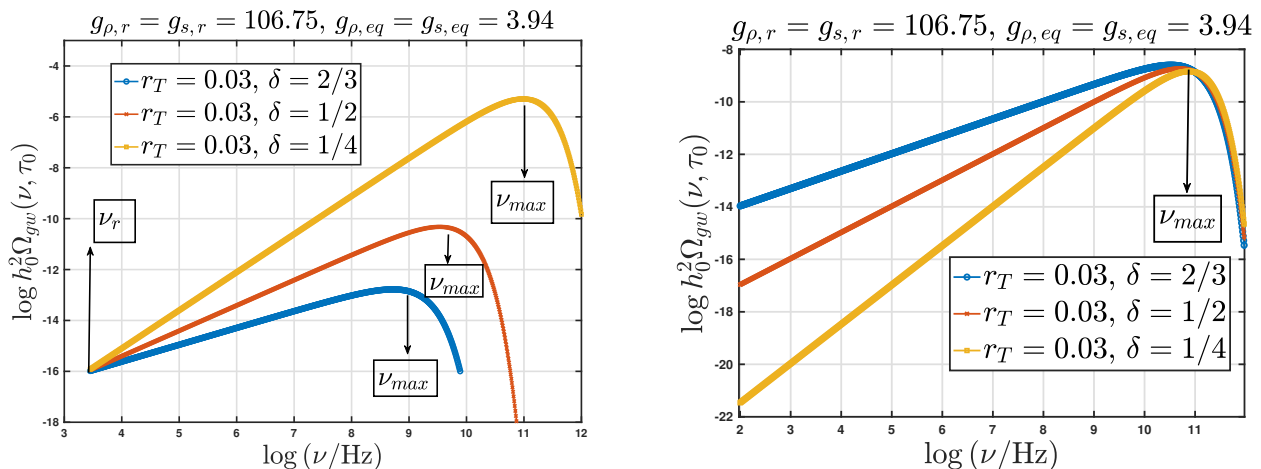


Figure 4: In the left plot the spectral energy density in critical units computed from Eqs. (4.14) and (4.28) is approximately normalized at ν_r , i.e. the lowest frequency compatible with the analytic treatment (see also Eq. (5.13)); different selections of the parameters are illustrated. In the right plot we instead normalize the same curves in the highest frequency domain compatible with the bounds of Eqs. (1.2) and (5.20).

rates δ_1 and δ_2 we have that ν_{max} becomes

$$\nu_{max} = \nu_1 = \prod_{i=1}^2 \xi_i^{\frac{\delta_i-1}{2(\delta_i+1)}} \bar{\nu}_{max} = \xi_1^{\frac{\delta_1-1}{2(\delta_1+1)}} \xi_2^{\frac{\delta_2-1}{2(\delta_2+1)}} \bar{\nu}_{max}, \quad (5.14)$$

where $\xi_1 = H_2/H_1$ and $\xi_2 = H_r/H_2$. The intermediate frequencies ν_2 and ν_r are related to $\bar{\nu}_{max}$ and they are

$$\begin{aligned} \nu_2 &= \sqrt{\xi_1} \xi_2^{(\delta_2-1)/[2(\delta_2+1)]} \bar{\nu}_{max}, \\ \nu_r &= \nu_3 = \sqrt{\xi_1} \sqrt{\xi_2} \bar{\nu}_{max} = \sqrt{\xi_r} \bar{\nu}_{max}, \end{aligned} \quad (5.15)$$

where, by definition, $\xi_r = \xi_1 \xi_2 = H_r/H_1$. Both Eqs. (5.14) and (5.15) can be generalized to the case of n intermediate stages of expansion [46].

5.3 The ultra-high frequency and the low frequency normalizations

In Eq. (1.2) it has been suggested that the upper bound on the frequency should be indeed of the order of the THz and this is what matters to set the absolute normalization in the ultra-high frequency regime. From a classical viewpoint the maximal frequency coincides with the minimal amplified wavelength of the spectrum and it ultimately depends on the post-inflationary evolution. This is, in a nutshell, the approach leading to Eqs. (3.35)–(3.36): ν_{max} gets modified depending upon the post-inflationary evolution. Equations (3.35)–(3.36) assume a single post-inflationary stage for curvature scales $H > H_r$ and this is why ν_{max} depends on δ , H_1 and H_r . A consequence of this observation is, for instance, that for the same value of the ratio $H_r/H_1 < 1$ the frequency ν_{max} is either larger or smaller than $\mathcal{O}(100)$ MHz depending if $\delta < 1$ or $\delta > 1$. Along a purely quantum mechanical perspective it is instead possible to derive an absolute upper bound on ν_{max} and while this analysis has been already presented in the recent past [22], it is now useful to deduce this bound in a slightly different manner. The first step is to express the spectral energy density in critical units in terms of the averaged multiplicity of the produced gravitons with opposite three-momenta:

$$\Omega_{gw}(\nu, \tau) = \frac{128 \pi^3}{3} \frac{\nu^4}{H^2 M_P^2 a^4} \bar{n}(\nu, \tau). \quad (5.16)$$

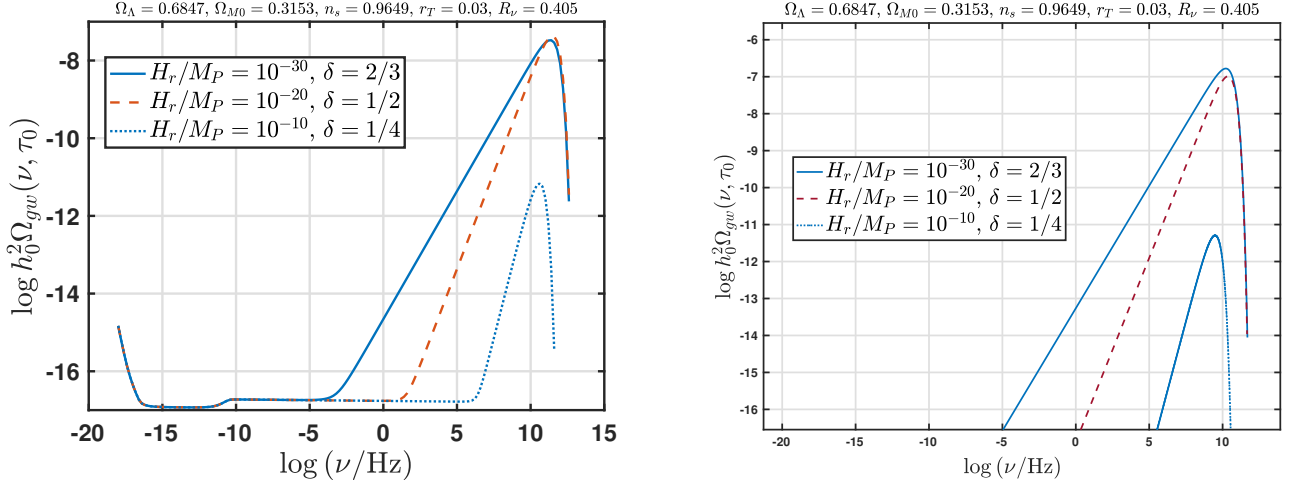


Figure 5: In the left plot the common logarithm of $h_0^2 \Omega_{gw}(\nu, \tau_0)$ is illustrated as a function of the common logarithm of the frequency. For both plots the post-inflationary expansion rate between H_1 and H_r is slower than radiation; the parameters involving the post-inflationary stage are the same in both plots. In the left plot the suppression below the nHz region comes predominantly from the free-streaming of the neutrinos. In the right plot we illustrate instead the analytic approximation (see Eqs. (4.14) and (4.28)) normalized in the high frequency domain.

Equation (5.16) suggests that the maximal frequency corresponds to the production a single pair relic gravitons: for frequencies smaller than ν_{max} the averaged multiplicity scales like a power-law while $\bar{n}(\nu, \tau_0)$ is exponentially suppressed for $\nu > \nu_{max}$. When only one pair is produced we have, from Eq. (5.16),

$$\Omega_{gw}(\nu, \tau_0) = \frac{128 \pi^3}{3} \frac{\nu_{max}^4}{H_0^2 M_P^2}. \quad (5.17)$$

Equation (5.17) sets already a generous limit on ν_{max} since $H_0 = 3.24 h_0 \text{ aHz}$ (we remind that $1 \text{ aHz} = 10^{-18} \text{ Hz}$) and $M_P = 1.855 \times 10^{31} \text{ THz}$: from the condition $\Omega_{gw}(\nu, \tau_0) < 1$ the maximal frequency must be already of the order of the THz but there is in fact a more constraining condition since the wavelengths reentering the Hubble radius between the end of inflation and big bang nucleosynthesis must comply with the bound

$$h_0^2 \int_{\nu_{bbn}}^{\nu_{max}} \Omega_{gw}(\nu, \tau_0) d \ln \nu < 5.61 \times 10^{-6} \left(\frac{h_0^2 \Omega_{\gamma 0}}{2.47 \times 10^{-5}} \right) \Delta N_\nu, \quad (5.18)$$

where $\Omega_{\gamma 0}$ is the (present) critical fraction of CMB photons and the integral at the left hand side of Eq. (5.18) must be evaluated, as indicated, between the frequency of big bang nucleosynthesis (i.e. ν_{bbn}) and ν_{max} .

Equation (5.18) sets an indirect constraint on the potential presence of extra-relativistic species at the time of nucleosynthesis [55, 56, 57]. Since Eq. (5.18) is also relevant in the context of neutrino physics the limit is often expressed in terms of ΔN_ν (i.e. the contribution of supplementary neutrino species). The constraints on ΔN_ν range from $\Delta N_\nu \leq 0.2$ to $\Delta N_\nu \leq 1$ so that the integrated spectral density in Eq. (5.18) must range, at most, between 10^{-6} and 10^{-5} . Given the expansion rate at the big bang nucleosynthesis time (when the temperature of the plasma was approximately $\mathcal{O}(1)$ MeV), ν_{bbn} can be expressed as:

$$\begin{aligned} \nu_{bbn} &= 8.17 \times 10^{-33} g_{\rho, bbn}^{1/4} T_{bbn} \left(\frac{h_0^2 \Omega_{R0}}{4.15 \times 10^{-5}} \right)^{1/4} \\ &= \mathcal{O}(2) \times 10^{-2} \left(\frac{g_{\rho, bbn}}{10.75} \right)^{1/4} \left(\frac{T_{bbn}}{\text{MeV}} \right) \left(\frac{h_0^2 \Omega_{R0}}{4.15 \times 10^{-5}} \right)^{1/4} \text{ nHz}. \end{aligned} \quad (5.19)$$

In a complementary perspective the diffuse background of relic gravitons was produced after BBN. In this case we observe that $\Omega_{gw}(\nu, \tau_0)$ must always be smaller than the the current fraction of relativistic species to avoid an observable impact on the CMB and matter power spectra [58, 59]. The two bounds are actually numerically compatible so that the final limit on ν_{max} is given by:

$$\nu_{max} \leq 0.165 \Omega_{R0}^{1/4} \sqrt{H_0 M_P} < \text{THz}, \quad (5.20)$$

where the inequality follows in the limit $\bar{n}(\nu_{max}, \tau_0) \rightarrow \mathcal{O}(1)$, i.e. in the case where a single pair of gravitons is produced. The bound of Eq. (5.20) is numerically more restrictive than the bounds derived from Eqs. (3.35) and (3.36) on the basis of classical considerations. We also stress that in Fig. 4 the upper curve of the left plot is not obviously compatible with the the bound of Eq. (5.18). This means that if we want to avoid the analysis of the low frequency domain of the spectrum, the analytic results for the spike should be mandatorily normalized by using the approach described in this subsection. The conclusions obtained from this strategy should not be interpreted as predictions but rather as upper bounds.

We are now going to consider more closely the interplay between the analytic results illustrated in the first part of this section and the numerical evaluation appropriately normalized at low frequencies [23, 53]. In this respect the first point to be stressed is that between the nHz domain and the audio band (with $\text{Hz} < \nu_{audio} < 10 \text{ kHz}$) the spectral energy density of inflationary origin is, at most, $\mathcal{O}(10^{-17})$ in critical units and the deviations from scale-invariance in the direction of blue spectral indices are excluded at least in the conventional situation where the corrections to $h_0^2 \Omega_{gw}(\nu, \tau_0)$ always lead to decreasing spectral slope [2, 3, 4]. The second relevant aspect is that, in the case of the concordance paradigm the spectral energy density is further reduced by various sources of damping and, most notably, by the free-streaming of neutrinos [31, 32, 33, 34, 35] operating below a fraction of the nHz. The same phenomenon also affects the spectral energy density when the corresponding slopes are increasing [30]; in both situations, however, the suppression due to the neutrinos operates for $\nu < \nu_{bbn}$ and when the expansion rate is already dominated by radiation. In Fig. 5 we illustrate a comparison between the analytic approximation normalized at the corresponding maximal frequency (see Eqs. (3.35)–(3.36)) and the full spectrum normalized at low frequency. The high frequency parameters of both plots are the same and we can see that, overall, the two results coincide within one order of magnitude both in the frequency domain and in the amplitude. In the aHz region the spectral energy density decreases as ν^{-2} while we can appreciate the suppression due to the neutrino free streaming close to ν_{bbn} [31, 32, 33, 34, 35]. Other sources of suppression taken into account in Fig. 5 and in the remaining plots include the late-time dominance of dark energy and the evolution of relativistic species. The spectra of Fig. 5 have been deduced by using for the fiducial parameters the last Planck data release in the case of three massless neutrinos where $R_\nu = \rho_\nu / (\rho_\gamma + \rho_\nu) = 0.405$, as indicated on top of each plots; this is the choice of the minimal Λ CDM scenario. If the radiation would dominate the whole post-inflationary evolution the quasi-flat plateau (decreasing because of the slow-roll corrections) would last up to frequencies $\mathcal{O}(300)$ MHz.

5.4 Absolute bounds on the post-inflationary expansion history

The analytic results Eqs. (4.14) and (4.28) leading to the right plot of Fig. 5 can also be employed to obtain more swiftly all the relevant bounds on the duration on the post-inflationary expansion rate. In the left plot of Fig. 6 we illustrated the bound of Eq. (5.18); the shaded area describes the region where the bound of Eq. (5.18) is satisfied. It is actually possible to distinguish two different shadings. The slightly larger area has been deduced by from the numerical result leading to the left plots of Fig. 5. The inner area has been instead obtained from the analytic approximation (see also the right plot of Fig. 5). The comparison of the two results shows that, as long as the ultra high frequency spikes are concerned, the approximation developed here is sufficiently accurate within an order of magnitude.

The bound of Eq. (5.18) is actually dominated by the highest frequencies of the spectrum and if we now move from the THz domain to the audio band the conclusions are quantitatively different but

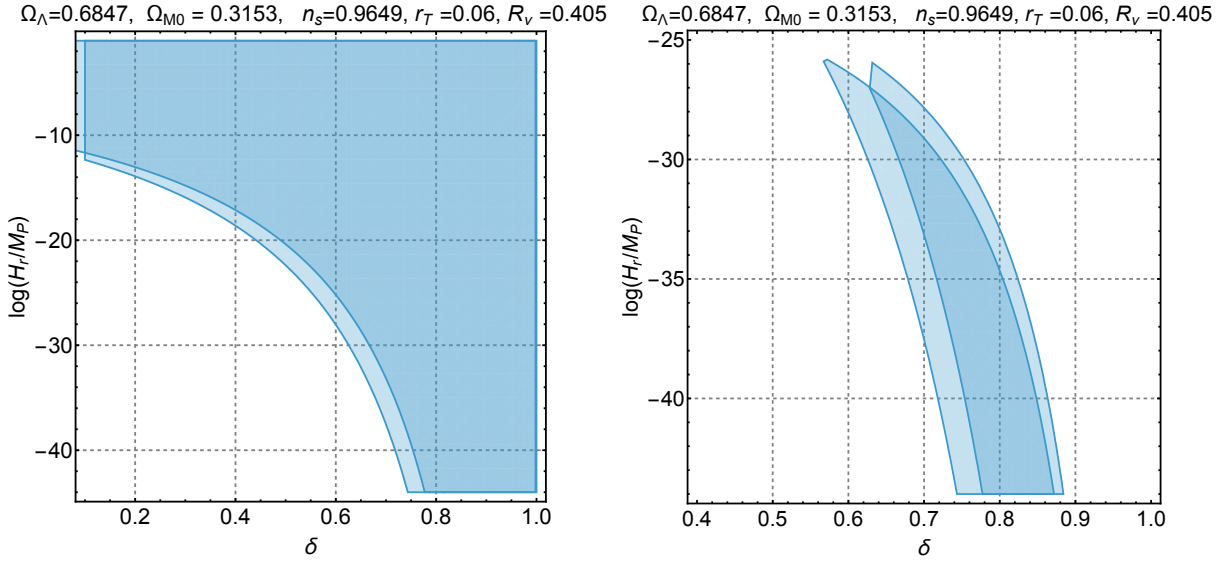


Figure 6: In the left plot the bound of Eq. (5.18) is illustrated in the plane $(H_r/M_P, \delta)$. The two shaded regions correspond to the approaches already scrutinized in Fig. 5. In the plot at the left the shaded areas denote the regions compatible with the BBN limit; in the right plot the BBN bound is combined with the requirement that the resulting signal is ultimately detectable in the audio band.

qualitatively very similar. For purposes of illustration the current limits on the presence of relic graviton backgrounds in the audio band [60, 61, 62, 63] (see also [5]) can be combined with a minimal requirement on the detectability of relic gravitons; we can then require

$$10^{-13} \leq h_0^2 \Omega_{gw}(\nu_{LVK}, \tau_0) < 10^{-10}, \quad \nu_{LVK} \leq \mathcal{O}(100) \text{ Hz}, \quad (5.21)$$

where ν_{LVK} denotes the Ligo-Virgo-Kagra frequency. The factor 10^{-13} is purely illustrative since we cannot foresee when the corresponding sensitivity will be reached by wide-band detectors. In the right plot of Fig. 6 the condition of Eq. (5.21) has been illustrated with the same logic pursued in the derivation of the left plot of the same figure. The two areas are practically superimposed; the rightmost region is obtained from the analytic approximation while the leftmost area follows from the numerical results.

5.5 Minimal detectable amplitudes and maximal frequencies

The analytic and numerical considerations developed in this paper allow for a direct estimate of the minimal chirp amplitudes required in the ultra-high frequency range for a direct detection of the cosmic gravitons. The minimal $h_c(\nu, \tau_0)$ resolved by a hypothetical detector should be at least twelve orders of magnitude smaller than the ones currently measured in the audio band, i.e. in the window ranging between few Hz and the kHz where wide-band detectors are currently operating. To clarify this statement the results obtained so far will now be used by normalizing the potential signal directly in the maximal frequency domain of the spikes. It is important to appreciate that the connection between the spectral energy density (in critical units) and the chirp amplitude $h_c(k, \tau_0)$ is well defined only when the relevant wavelengths are shorter than the Hubble radius and this is because the chirp amplitude is proportional to the tensor power spectrum $P_T(k, \tau)$. Indeed the chirp amplitude is simply defined as:

$$\langle \hat{h}_{ij}(\vec{x}, \tau) \hat{h}^{ij}(\vec{x}, \tau) \rangle = 2h_c^2(\vec{x}, \tau) = 2 \int \frac{dk}{k} h_c^2(k, \tau) j_0(kr), \quad (5.22)$$

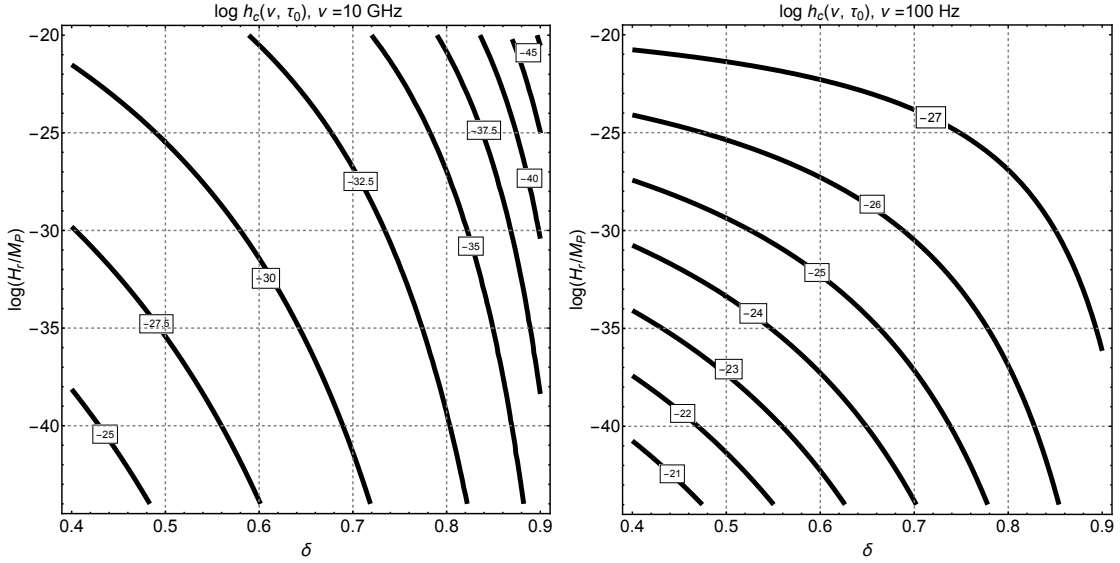


Figure 7: The values of the chirp amplitudes in the plane $(H_r/M_P, \delta)$ are illustrated for two typical (comoving) frequencies. The labels appearing on the contours denote the common logarithms of the chirp amplitudes at the frequencies of 10 GHz (left plot) and of 100 Hz (right plot). As ν increases the minimal chirp amplitudes potentially measured by a hypothetical high frequency instrument must be reduced in comparison with the $h_c^{(min)}(\nu, \tau_0)$ that can be currently measured in audio band. Depending on the value of the comoving frequency the minimal chirp amplitude should be 12 or even 14 orders of magnitude smaller than the ones now associated with a signal in the region of 0.1 kHz.

where, as usual, $j_0(kr)$ is the spherical Bessel function of zeroth order. By now recalling Eqs. (2.6) and (2.9) we obtain from Eq. (5.22)

$$\langle \hat{h}_{ij}(\vec{k}, \tau) \hat{h}_{mn}(\vec{p}, \tau) \rangle = \frac{4\pi^2}{k^3} h_c^2(k, \tau) \mathcal{S}_{ijmn}(\hat{k}) \delta^{(3)}(\vec{k} + \vec{p}), \quad (5.23)$$

which also means that $P_T(k, \tau) = 2h_c^2(k, \tau)$. Equations (5.22)–(5.23) implicitly suggest that the only way to obtain a connection between $h_c^2(k, \tau)$ and the spectral energy density of Eq. (2.14) is consider, as anticipated, typical wavelengths shorter than the Hubble radius; in this case we obtain

$$\Omega_{gw}(k, \tau) = \frac{k^2}{6H^2 a^2} h_c^2(k, \tau), \quad Q_T(k, \tau) \simeq k^2 P_T(k, \tau), \quad (5.24)$$

where the second (approximate) equation is only valid when the corresponding wavelengths are shorter than the Hubble radius. If we now switch from the comoving wavenumber to the comoving frequency we obtain from Eq. (5.24), at the present time,

$$\Omega_{gw}(\nu, \tau_0) = \frac{2\pi^2}{3} \left(\frac{\nu}{H_0} \right)^2 h_c^2(\nu, \tau_0) = 1.27 \left(\frac{h_0}{0.7} \right)^{-2} \left(\frac{\nu}{\text{aHz}} \right)^2 h_c^2(\nu, \tau_0). \quad (5.25)$$

Equation (5.25) already explains, in a rather qualitative manner, why the chirp amplitude associated with cosmic gravitons should be rather minute in the ultra-high frequency range.

From Eq. (5.24) it is useful to deduce a direct relation between the chirp amplitude and the averaged multiplicity in the ultra-high frequency domain:

$$h_c(\nu, \tau_0) = 7.643 \times 10^{-34} \left(\frac{\nu}{\text{GHz}} \right) \sqrt{\bar{n}(\nu, \tau_0)}. \quad (5.26)$$

Since, by definition, around the maximal frequency the averaged multiplicity is $\mathcal{O}(1)$, the largest spectral domain is only be accessible when $h_c^{(min)}(\nu, \tau_0)$ is smaller (or even much smaller) than $\mathcal{O}(10^{-22})$. We also know that the averaged multiplicity scales as $(\nu/\nu_{max})^{-4+n_T}$; from Eq. (5.26) it follows

$$h_c^{(min)}(\nu, \tau_0) < 8.13 \times 10^{-32} \left(\frac{\nu}{0.1 \text{ THz}} \right)^{-1+n_T/2}. \quad (5.27)$$

In Fig. 7 the labels on the contours correspond to the common logarithm of the chirp amplitude in the plane $(H_r/M_P, \delta)$. In the left plot the typical frequency has been chosen to be 10 GHz while in the right plot the frequency falls in the audio band. From the comparison between the two plots we can argue that the the minimal detectable $h_c(\nu, \tau_0)$ at high and intermediate frequencies: to require the same $h_c^{(min)}(\nu, \tau_0)$ both in the audio and in the THz bands makes no sense. The same argument could be phrased also in terms of the spectral energy density since we know that

$$h_c(\nu, \tau_0) = 1.263 \times 10^{-20} \left(\frac{100 \text{ Hz}}{\nu} \right) \sqrt{h_0^2 \Omega_{gw}(\nu, \tau_0)}. \quad (5.28)$$

From Eq. (5.28) the chirp amplitude can be directly deduced from the analytic determinations of $\Omega_{gw}(\nu, \tau_0)$ and this is what has been done in Fig. 7.

All in all, a sensitivity $\mathcal{O}(10^{-20})$ or even $\mathcal{O}(10^{-24})$ in the chirp amplitude between the MHz and the THz regions is immaterial for ultra-high frequency gravitons. It has been suggested in the past that microwave cavities [13, 14, 15, 16, 17, 18] operating in the MHz and GHz regions should be employed for the detection of relic gravitons [10] (see also [18]). The relic signal is rather unique for its deep theoretical implications that are probably more relevant than the discovery of a new source of gravitational radiation. These instruments have been also suggested in a series of interesting studies in Refs. [64, 65, 66, 67] by setting the required chirp amplitudes in the range $h_c^{(min)}(\nu, \tau_0) = \mathcal{O}(10^{-20})$ for arbitrarily high frequencies. As suggested in Fig. 7 a minimal chirp amplitude $h_c^{(min)}(\nu, \tau_0) = \mathcal{O}(10^{-20})$ is more than 10 orders magnitude larger than the requirements associated with the direct detection of cosmic gravitons. Equations (5.27)–(5.28) also clarify why $h_c^{(min)}(\nu, \tau_0)$ must be at least $\mathcal{O}(10^{-32})$ (or smaller) for a potential detection of cosmic gravitons in the THz domain. We should however note that while for $n_T > 2$ the largest signal occurs at the largest frequency, for $n_T \leq 2$ the signal may increase for frequencies smaller than the THz are. If we consider, for instance, the case $n_T \rightarrow 1$ we would have that the chirp amplitude in the MHz range could be $\mathcal{O}(10^{-28})$ (this is why this case was regarded as particularly interesting in Refs. [17, 18]). Furthermore, when $n_T \rightarrow 2$ we would have instead that $h_c(\nu, \tau_0)$ is the same at higher and smaller frequencies. Finally for $n_T \rightarrow 3$ the chirp amplitude at lower frequencies is even more suppressed. There is a non-trivial interplay between the optimal frequency, the features of the signal and the noises (especially the thermal one) indicating that the ultra-high frequency (close to ν_{max}) is not always the most convenient. This aspect should probably be taken into account if the goal is really an accurate assessment of the required sensitivities associated with promising (but still hypothetical) high frequency instruments.

6 Concluding remarks

The reliable evaluations of the potential signals associated with the ultra-high frequency gravitons must encompass the whole spectrum ranging between few aHz and the THz region. On the one hand the current limits and the known damping sources in the aHz and nHz domains are essential for the analysis of the concordance paradigm and of its neighbouring extensions. On the other hand the production of few pairs of gravitons with opposite three-momenta defines operationally the maximal spectral frequency falling in the THz range. In this broad interval consisting of more than three decades in frequency, the spectral energy density and the averaged multiplicities of the relic gravitons may offer, in the years to come, a *prima facie* evidence of the early expansion history of the Universe. Both the presence and the absence of cosmic gravitons domain shall be extremely relevant provided these phenomena are investigated with the appropriate sensitivities: artificially reducing the demands on the minimal sensitivities, especially at high frequencies, does not usually offer any effective shortcut to swift discoveries.

Although below the nHz various sources of suppression concurrently reduce the spectral energy density, we found useful to scrutinize the approximate estimates of the high frequency spikes that may potentially develop between the THz and $\mathcal{O}(300)\sqrt{H_r/H_1}$ MHz where $H_r \geq 10^{-44} M_P$ (as implied by the tests on the expansion history at the onset of big bang nucleosynthesis) and $H_1 = \mathcal{O}(10^{-6}) M_P$. Along this perspective a number of complementary computational schemes have been introduced with the purpose of assessing their mutual accuracy in comparison with more faithful numerical analyses also accounting for the low frequency effects. We first examined the WKB approach together with various strategies based on the analysis of the transition matrix that relates the evolution of the mode functions between the inflationary and the post-inflationary stages of evolution. Even though between H_1 and H_r various intermediate epochs may appear, in this investigation we simply considered the presence of a single post-inflationary stage preceding the conventional radiation-dominated phase. Exactly the same procedure illustrated here can be however extended to more general situations where the post-inflationary evolution includes different expanding stages. It turns out that the general bounds on the post-inflationary expansion rate can be swiftly deduced with the analytic approach developed in this investigation and they compare quite well with more accurate strategies including the sources of late-time suppression of the spectrum.

For a direct detection of a cosmic signal in the ultra-high frequency band, the present estimates confirm that the required sensitivity in the chirp amplitude should be at least twelve or even thirteen orders of magnitude smaller than the ones currently accessible between few Hz and the kHz where the wide band interferometers are currently taking data. If electromechanical detectors (e.g. microwave cavities) operating between the MHz and the THz will ever be able to achieve these sensitivities, the timeline of the post-inflationary expansion rate might be observationally accessible in the years to come. As repeatedly suggested in the past, this perspective encourages a synergic approach between experiments scrutinizing different branches of the graviton spectrum at low, intermediate and ultra-high frequencies. It would actually seem rather bizarre to set the detectability strategies for ultra-high frequencies by deliberately disregarding the motivated physical properties of the largest cosmic signal between the MHz and the THz.

Acknowledgements

It is also a pleasure to thank A. Gentil-Beccot, A. Kohls, L. Pieper, S. Rohr and J. Vigen of the CERN Scientific Information Service for their kind help.

References

- [1] S. Weinberg, *Cosmology* (Oxford University Press, Oxford, UK, 2008).
- [2] Y. Akrami *et al.* [Planck Collaboration], *Astron. Astrophys.* **641**, A10 (2020).
- [3] N. Aghanim *et al.* [Planck Collaboration], *Astron. Astrophys.* **641**, A6 (2020).
- [4] P. Ade *et al.* [BICEP and Keck], *Phys. Rev. Lett.* **127**, 151301 (2021).
- [5] M. Giovannini, *Prog. Part. Nucl. Phys.* **112**, 103774 (2020).
- [6] L. P. Grishchuk, *Sov. Phys. JETP* **40**, 409 (1975) [*Zh. Eksp. Teor. Fiz.* **67**, 825 (1974)].
- [7] L. P. Grishchuk, *Annals N. Y. Acad. Sci.* **302**, 439 (1977).
- [8] A. A. Starobinsky, *JETP Lett.* **30**, 682 (1979) [*Pisma Zh. Eksp. Teor. Fiz.* **30**, 719 (1979)].
- [9] V. A. Rubakov, M. V. Sazhin and A. V. Veryaskin, *Phys. Lett. B* **115**, 189 (1982).
- [10] M. Giovannini, *Phys. Rev. D* **58**, 083504 (1998).
- [11] V. B. Braginsky and M. B. Menskii, *Pis'ma Zh. Eksp. Teor. Fiz.* **13**, 585 (1971) [*JETP Lett.* **13**, 417 (1971)].
- [12] V. B. Braginsky, L.P. Grishchuk, A. G. Doroshkevich, Ya. B. Zeldovich, I. D. Novikov and M. Sazhin, *Sov. Phys. JETP* **38**, 865 (1974) [*Zh. Eksp. Teor. Fiz.* **65**, 1729 (1973)].
- [13] F. Pegoraro, L. Radicati, Ph. Bernard, and E. Picasso, *Phys. Lett. A* **68**, 165 (1978); F. Pegoraro, E. Picasso, and L. Radicati, *J. Phys. A* **11**, 1949 (1978); E. Iacopini, F. Pegoraro, E. Picasso, and L. Radicati, *Phys. Lett. B* **73**, 140 (1979).
- [14] C. M. Caves, *Phys. Lett. B* **80**, 323 (1979).
- [15] C. Reece, P. Reiner, and A. Melissinos, *Phys. Lett. A* **104**, 341 (1984); *Nucl. Inst. and Methods, A* **245**, 299 (1986).
- [16] Ph. Bernard, G. Gemme, R. Parodi and E. Picasso, *Rev. Sci. Instrum.* **72**, 2428 (2001).
- [17] R. Ballantini, P. Bernard, A. Chincarini, G. Gemme, R. Parodi and E. Picasso, *Class. Quant. Grav.* **21**, S1241 (2004).
- [18] M. Giovannini, *Phys. Rev. D* **60**, 123511 (1999); *Class. Quant. Grav.* **16**, 2905 (1999).
- [19] A. M. Cruise, *Class. Quantum Grav.* **17**, 2525 (2000); A. M. Cruise and R. Ingle, *Class. Quantum Grav.* **22**, S479 (2005); *Class. Quantum Grav.* **23**, 6185 (2006).
- [20] F. Li, M. Tang and D. Shi, *Phys. Rev. D* **67**, 104008 (2003); F. Li, Z. Wu and Y. Zhang, *Chin. Phys. Lett.* **20**, 1917 (2003).
- [21] A. Nishizawa *et al.*, *Phys. Rev. D* **77**, 022002 (2008); A. T. Akutsu *et al.*, *Phys. Rev. Lett.* **101**, 101101 (2008).
- [22] M. Giovannini, *Phys. Lett. B* **854**, 138769 (2024); *Phys. Rev. D* **110**, 123520 (2024); *JCAP* **05**, 056 (2023).
- [23] M. Giovannini, *Phys. Rev. D* **108**, 123508 (2023); *Phys. Rev. D* **111**, L061301 (2025).
- [24] L. Parker, *Phys. Rev. Lett.* **21**, 562 (1968).
- [25] L. Parker, *Phys. Rev.* **183**, 1057 (1969).
- [26] N. D. Birrel and P. C. W. Davies, *Quantum fields in curved spaces* (Cambridge Univ. Press, Cambridge, England, 1982).
- [27] L. Parker and D. Toms, *Quantum Field Theory in Curved Space-time*, (Cambridge University Press, Cambridge 2009).
- [28] E. D. Schiappacasse and L. H. Ford, *Phys. Rev. D* **94**, 084030 (2016)
- [29] L. H. Ford, *Rept. Prog. Phys.* **84**, 116901 (2021)
- [30] M. Giovannini, *Phys. Lett. B* **668**, 44 (2008); *Class. Quant. Grav.* **26**, 045004 (2009).

- [31] S. Weinberg, Phys. Rev. D **69**, 023503 (2004).
- [32] D. A. Dicus and W. W. Repko, Phys. Rev. D **72**, 088302 (2005).
- [33] H. X. Miao and Y. Zhang, Phys. Rev. D **75**, 104009 (2007).
- [34] B. A. Stefanek and W. W. Repko, Phys. Rev. D **88**, 083536 (2013).
- [35] K. W. Ng, Phys. Rev. D **86**, 103510 (2012).
- [36] L. H. Ford and L. Parker, Phys. Rev. D **16**, 1601 (1977).
- [37] M. A. H. MacCallum and A. H. Taub, Commun. Math. Phys. **30**, 153 (1973).
- [38] L. D. Landau and E. M. Lifshitz, *The Classical Theory of Fields*, (Pergamon Press, New York, 1971).
- [39] D. R. Brill and J. B. Hartle, Phys. Rev. **135**, B271 (1964).
- [40] R. A. Isaacson, Phys. Rev. **166**, 1263 (1968); Phys. Rev. **166**, 1272 (1968).
- [41] S. V. Babak and L. P. Grishchuk, Phys. Rev. D **61**, 024038 (2000).
- [42] L. M. Butcher, A. Lasenby and M. Hobson, Phys. Rev. D **78**, 064034 (2008).
- [43] L. M. Butcher, M. Hobson and A. Lasenby, Phys. Rev. D **80**, 084014 (2009).
- [44] M. Giovannini, Phys. Rev. D **100**, 083531 (2019).
- [45] M. Giovannini, JCAP **11**, 027 (2024).
- [46] M. Giovannini, [arXiv:2412.13968 [gr-qc]].
- [47] A. Erdelyi, W. Magnus, F. Oberhettinger, and F. R. Tricomi *Higher Transcendental Functions* (Mc Graw-Hill, New York, 1953).
- [48] M. Abramowitz and I. A. Stegun, *Handbook of Mathematical Functions* (Dover, New York, 1972).
- [49] M. S. Turner, Phys. Rev. D **28**, 1243 (1983).
- [50] C. Pathinayake and L. H. Ford, Phys. Rev. D **35**, 3709 (1987).
- [51] L. H. Ford, Phys. Rev. D **35**, 2955 (1987).
- [52] J. D. Barrow, Phys. Rev. D **48**, 1585 (1993).
- [53] M. Giovannini, Phys. Rev. D **105**, 103524 (2022).
- [54] L. Parker, Nature **261**, 20 (1976).
- [55] V.F. Schwartzman, Pis'ma Zh. Eksp. Teor. Fiz. **9**, 315 (1969) [JETP Lett. **9**, 184 (1969)].
- [56] M. Giovannini, H. Kurki-Suonio and E. Siuhvola, Phys. Rev. D **66**, 043504 (2002).
- [57] R. Cyburt, B. D. Fields, K. A. Olive, and E. Skillman, Astropart. Phys. **23**, 313 (2005).
- [58] T. L. Smith, E. Pierpaoli and M. Kamionkowski, Phys. Rev. Lett. **97**, 021301 (2006).
- [59] D. M. Siegel and M. Roth, Astrophys. J. **784**, 88 (2014).
- [60] B. Abbott *et al.* [LIGO Collaboration], Phys. Rev. D **69**, 122004 (2004); Phys. Rev. Lett. **95**, 221101 (2005).
- [61] J. Aasi *et al.* [LIGO/Virgo Collaboration], Phys. Rev. Lett. **113**, 231101 (2014); Phys. Rev. D **91**, 022003 (2015).
- [62] B. P. Abbott *et al.* [LIGO/Virgo Collaboration], Phys. Rev. Lett. **118**, 121101 (2017) Erratum: [Phys. Rev. Lett. **119**, 029901 (2017)]; Phys. Rev. D **100**, 061101(R) (2019).
- [63] R. Abbott *et al.* [KAGRA, Virgo and LIGO Scientific], Phys. Rev. D **104**, 022004 (2021).
- [64] Y. Kahn, B. R. Safdi, and J. Thaler, Phys. Rev. Lett. **117**, 141801 (2016).
- [65] S. Chaudhuri, P. W. Graham, K. Irwin, J. Mardon, S. Rajendran and Y. Zhao, Phys. Rev. D **92**, 075012 (2015).
- [66] J. L. Ouellet *et al.*, Phys. Rev. Lett. **122**, 121802 (2019).
- [67] R. Lasenby, Phys. Rev. D **102**, 015008 (2020).